INSTITUTE OF PHYSICS PUBLISHING PLASMA SOURCES SCIENCE AND TECHNOLOGY
Plasma Sources Sci. Technol. **11** (2002) 525–543 PII: S0963-0252(02)54581-3

Electron energy distribution function measurements and plasma parameters in inductively coupled argon plasma

V A Godyak, R B Piejak and B M Alexandrovich

OSRAM SYLVANIA, 71 Cherry Hill Drive, Beverly, MA 01915, USA

E-mail: valery.godyak@sylvania.com

Received 7 May 2002, in final form 8 October 2002
Published 8 November 2002
Online at stacks.iop.org/PSST/11/525

Abstract
Electron energy distribution functions (EEDFs) have been measured in a cylindrical inductively coupled plasma (ICP) with a planar coil over a wide range of external parameters (argon pressure, discharge power and driving frequency). The measurements were performed under well-defined discharge conditions (discharge geometry, rf power absorbed by plasma, external electrical characteristics and electromagnetic field and rf current density profiles). Problems found in many probe measurements in ICPs were analysed and a rationale for designing probe diagnostics that addresses these problems is presented in this paper. A variety of plasma parameters, such as, plasma density, effective and screen electron temperatures, electron–atom transport collision frequency, effective rf frequency and rates of inelastic processes, have been found as appropriate integrals of the measured EEDFs. The dependence of these ICP parameters over a wide range of argon pressure, rf power and frequency results in experimental scaling laws that are suitable for comparison with ICP models and helpful in ICP design for many applications.

1. Introduction

Inductively coupled plasma (ICP) sources or inductive discharges have been known for over a century. They have been used and studied in past decades mostly in two quite opposite regimes. At high gas pressure (about atmospheric pressure) ICPs produce plasma that is near equilibrium, while at low-pressure (mTorr range) ICPs produce non-equilibrium plasmas. Low-pressure ICPs have been used as ion sources for particle accelerators and as ion thrusters for space propulsion. Recently, interest in low-pressure ICPs has been revitalized due to their great promise in plasma processing and lighting technology. The capability to provide a large plasma density at a low gas pressure and the absence of electrodes has made these discharges attractive in development of new technology and has stimulated intensive research activity on basic plasma phenomena occurring in such discharges.

The ICP is maintained by alternating current in a coil surrounding, or immersed in, a discharge chamber. The alternating current produces a time-varying magnetic field, which induces an electric field according to Faraday's law. The lines of electric field close upon themselves and are parallel to the coil turns, thus producing similarly directed rf current in the plasma. In an ICP the absence of rf electrodes with high rf voltage removes many of the constraints associated with rf sheaths in capacitively coupled plasmas.

ICP sources are the most energy efficient yet cost effective way to produce high-density plasma at low gas pressure. Compared with microwave (ECR and helicon) plasma sources, ICPs do not require a dc magnetic field and expensive microwave equipment. RF power sources for ICP operate at frequencies between hundreds of kilohertz and a few megahertz and are more efficient and less expensive than microwave power sources.

In an ICP the main interaction between an electromagnetic field and the plasma, and thus rf power dissipation, takes place in the skin layer near the plasma boundary. Depending on plasma size, gas pressure and driving frequency, various interactions between the electromagnetic field and the plasma may occur.

Non-local coupling of the electron energy distribution function (EEDF) and its scalar integrals with the rf electric field (non-local electron kinetics) is well recognized as an underlying feature of low-pressure rf discharges. Due to a large electron thermal conductivity, the electron energy relaxation length is larger than the plasma size and the spatial distribution of plasma parameters is practically independent of the distribution of the rf heating field.

In the mTorr pressure range, when the characteristic scale of the electromagnetic field is smaller than an electron mean free path, non-local electrodynamics effects due to electron thermal motion may play an essential role in ICP operation. Under such conditions the rf current in the ICP is not locally coupled with the rf field (anomalous skin effect), resulting in a non-monotonic space distribution of rf field and rf current, collisionless electron heating and negative power absorption.

At a low driving frequency, requiring a relatively large rf magnetic field to induce a sustaining rf electric field, the rf Lorentz force acting on electrons in the ICP skin layer prevails over the rf electric force and electromagnetic field interaction with the plasma becomes non-linear. Second harmonic polarization potential in the skin layer, second harmonic current circulating around the main discharge current at the fundamental frequency and modification of the plasma density and ambipolar profile by ponderomotive force are typical in the non-linear regime.

One objective of the present study is to generate a comprehensive experimental database of ICP plasma parameters over a wide range of discharge conditions (power, gas pressure and frequency) covering collisional, collisionless (stochastic) and non-linear ICP regimes. From this database, empirical scaling laws can be deduced. Scaling laws are of paramount importance in designing a practical ICP device and are an effective lever to control and optimize device performance. In addition, the database can serve to verify numerical modelling (virtual experiments) to establish their practical use.

There have been many recent attempts to measure electrical and plasma characteristics of ICPs. Various parameters were obtained in various configurations and sizes, for different gas types at various gas pressures and driving frequencies. Unfortunately, it is difficult to conclusively determine ICP scaling laws from these many measurements because ICP characteristics are device specific; most of these measurements were made over a narrow parameter space and, in many cases, the quality of the measurements is questionable.

To measure a mutually compatible set of ICP parameters, measurements should be done under the same discharge conditions, in the same discharge chamber and preferably using the same sustaining and diagnostic means. To achieve this end, we have designed a discharge chamber with geometry that is convenient for analysis and suitable for reliable Langmuir and magnetic probe diagnostics. In designing this experimental setup, we have followed the concept of adjusting the discharge to the diagnostics rather than adjusting the diagnostics to the discharge.

The paper is organized as follows. Section 2 is a concise review of recent works on probe measurements in an argon ICP. This is followed by a discussion of typical problems in probe diagnostics in high-density, and in particular, inductive plasmas (section 3). In section 4, we analyse probe measurement circuits and give a rationale for probe experiment design in high-density plasmas. Experimental results carried out over a wide range of discharge conditions and a discussion of experimental scaling laws for argon ICP is presented in section 5. The final part of this work is a short summary with conclusions.

2. Recent works on probe measurements in ICP

Many works have been published in recent years on Langmuir probe diagnostics in argon ICP sources. Hopwood *et al* [1] have measured plasma density, electron temperature and plasma potential over a wide range of argon pressure between 0.3 and 30 mTorr in a cylindrical ICP with a planar coil. In this work, plasma density was found from the ion part of the probe characteristic using the Bohm formula for ion current to a cylindrical probe, assuming an infinitely small probe sheath. Electron temperature and plasma potential were found using a standard Langmuir procedure assuming a Maxwellian EEDF. These authors found a monotonic drop in electron temperature with argon pressure and a monotonic rise in plasma density with gas pressure and power. These trends in plasma parameter versus gas pressure are typical for low-pressure gas discharges and follow from the ionization and energy balances in bounded discharge plasma. Due to the assumption of a Maxwellian EEDF and use of the Bohm expression for ion current to the probe, these results [1] should be considered as qualitative. However, this work seems to be the first attempt to experimentally determine scaling laws for ICP basic parameters.

Mahoney *et al* [2] have measured EEDFs over an ICP volume and found considerable change in the average electron energy. They also observed ripples on the EEDF (growing with discharge power) and have interpreted them as a population of cold electrons. A significant discrepancy in plasma density found from electron and ion parts of the probe characteristic was reported there.

Detailed space-resolved EEDF measurements in an ICP with a flat coil, were performed by Kortshagen *et al* [3]. They found a transition in EEDF shape in the elastic energy range, from a concave curvature at low argon pressure to a convex curvature at high pressure. Generally, good agreement was found between experiments at low argon pressure and theoretical predictions of a three-temperature EEDF based on non-local electron kinetics. Limited EEDF measurement resolution at low electron energy accounted for a discrepancy at higher argon pressure ($p \geqslant 10$ mTorr) where a Druyvesteyn-like distribution was measured. An asymmetrical axial plasma profile has been found at this pressure and was interpreted to be a consequence of different boundary conditions on the window and metallic wall of the discharge chamber [4]. More accurate EEDF measurement, made by Mumken [5], has shown a Maxwellian distribution in the elastic energy range at higher argon pressure and proved that asymmetry in the axial plasma distribution results from violation of EEDF non-locality in the inelastic energy range.

EEDF measurements over a wide range of rf power and argon pressure in an ICP with a planar coil have been reported by Godyak [6, 7]. A high-energy tail in the inelastic energy

range of the EEDF and a low energy peak was found at the discharge centre at low argon pressure, but the relative population of low energy electrons was found to be much larger than in previous works. In contrarst to [2], the low energy peak of the EEDF disappeared at higher discharge power. At relatively high argon pressure and high discharge power, the EEDF in elastic energy range, in contradiction with results of [3] (and many others), was found to be Maxwellian. A small anisotropy in the EEDF within the skin layer was found at 1 mTorr argon pressure, while behind the skin layer the EEDF was quite isotropic. An asymmetric axial plasma density distribution (similar to that in [3] and [5]) was obtained in [7] in a 10 mTorr ICP.

EEDFs and plasma parameters in alternative ICP devices, having a geometry different from that of a simple cylinder with a planar coil, were measured by Godyak *et al* [8] in a coaxial cylindrical ICP with an internal coil and by Schwabedissen *et al* [9] in a GEC Reference Cell modified for ICP operation. These authors also have measured EEDFs in a variety of noble gases like helium, neon, krypton and xenon.

A considerable number of EEDF measurements in argon ICP were made in recent years in different experimental setups. Many of these have demonstrated the non-local nature of electron kinetics in low-pressure ICPs [3, 5, 9, 10], where the EEDF as a function of the total (kinetic plus potential) electron energy was found to be spatially uniform. This EEDF feature is inherent to any kind of low-pressure discharge (dc, rf or microwave), independent of the specific electron heating mechanism, as long as the electron energy relaxation length λ_ε is much larger than the characteristic plasma size Λ defined by the shortest discharge dimension. For a shallow cylindrical discharge with height $L \ll 2R$, $\Lambda = L/2$. On the other hand, at 10 mTorr and above, where λ_ε is approaching Λ, the electrons tend to exhibit local behaviour in the high-energy tail of the EEDF, corresponding to an inelastic energy range ($\varepsilon > \varepsilon^*$, where ε^* is the electron excitation energy). Experiments [5, 11] have demonstrated an essential increase in the EEDF tail temperature measured in the ICP skin layer, where a strong rf induction field was localized.

The frequency dependence of an EEDF in a low-pressure ICP under conditions of anomalous skin effect was studied in [12]. At low rf power the effective electron temperature in the measured EEDF was found to have a three-temperature structure with temperature falling with driving frequency. At high rf power (large plasma density), the measured EEDFs in elastic energy range ($\varepsilon < \varepsilon^*$) evolved into a Maxwellian distribution with temperature independent of frequency.

Modification of the EEDF [13] and plasma parameter spatial distribution [14] by ponderomotive force, caused by the very rf magnetic field that maintains the discharge, has been studied in a low-pressure ICP operating at low frequency. A significant depletion of the low energy part of the measured EEDF and a corresponding reduction in plasma density within the skin layer have been found in these experiments.

Axial and radial plasma parameter distributions were studied in argon ICP with a flat coil in [3, 5] and recently in helium ICP [15]. In all of these works a distribution typical of bounded plasma, consisting of a monotonic drop in the plasma density near the chamber wall, was found. Plausible agreement was demonstrated between the experimental plasma density distribution and that calculated from a fluid approximation.

Different results were obtained in [16] using probe techniques in an argon ICP with a flat coil operating at 0.5 MHz in the range of argon pressure between 0.3 and 900 mTorr. In this work, a uniform plasma density distribution was measured along the axial and radial directions over much of the discharge chamber. Over this pressure range, the authors found an essentially constant electron temperature and power independent of plasma density in an inductive mode. The apparent inconsistency of these results with the ionization and energy balance of the gas discharge plasma brings the validity of the probe diagnostics in this experiment into question.

3. Problems found in ICP probe diagnostics

3.1. Poorly defined discharge conditions

Prior to a discussion of typical problems encountered in probe diagnostics in ICPs, let us consider some general issues that reduce the usefulness of ICP diagnostics found in many industrial and laboratory ICP experiments. One issue is uncertainty in the discharge condition, due to a poorly defined plasma geometry (like in GEC Reference Cell, where plasma volume depends on rf power, gas type and pressure) and more often, due to poorly defined rf power delivered to the plasma. Terms like 'ICP power', 'applied power', 'transmitted power', 'system power', 'nominal power', etc frequently, without definition, can be seen in the literature, while only power consumed by the plasma itself is relevant to the measured plasma parameters.

In characterization of an ICP by power, the transmitted (incident minus reflected) rf power P_t, fed to an ICP inductor coil and measured in a 50 Ω line between the rf power source and the resonant matching network, is often given. The transmitted power P_t consists of the power dissipated in the plasma P_d, as well as, power P_m dissipated in the inductor coil, in the metal chamber wall (due to induced rf currents there) and in different parts of the resonant matching circuit, including connectors, wire leads and cables, $P_t = P_d + P_m$. Unfortunately, the rf power P_d delivered to the plasma is always smaller than the transmitted power P_t. Power transfer efficiency of an ICP, defined as P_d/P_t, usually ranges between 10% and 90%. P_d/P_t is lowest for low gas pressure, in molecular and electro-negative gases and at low discharge power. As a rule, P_d/P_t grows with discharge power and gas pressure and is larger for ICP systems with a higher Q-factor of the unloaded inductor coil and with closer coupling between the coil and plasma [17, 18]. Since power transfer efficiency changes with discharge power, the rf power dissipated in the plasma is not generally proportional to the transmitted power. Plasma parameters measured at a fixed transmitted, or incident rf power, have limited value since they cannot be related to the specific rf power delivered to the plasma.

Another issue to consider in ICP systems is capacitive coupling between the inductor coil and the plasma. Although, in the inductive mode, rf power deposition due to capacitive coupling is negligible, the latter can significantly affect plasma parameters of an ICP due to ion bombardment of the dielectric window separating the induction coil and the plasma. This may occur in various ways: by plasma contamination with sputtered window material, and/or by secondary γ-electrons, induced from ions accelerated in the rf sheath between the

window and the plasma, bombarding the window. Similar to a capacitive discharge in the γ-mode, a very small amount of the γ-electrons, induced by the capacitive coupling, can essentially change the plasma density and the electron temperature of ICP. Capacitive coupling in an ICP also leads to significant rf plasma potential, thus, complicating plasma diagnostics with Langmuir and/or magnetic probes, since special means are required to mitigate the rf voltage across the probe sheath and common mode pickup of a magnetic probe. Screening the inductor coil [18] and/or use of a symmetric (push–pull) circuits [19, 20] allows for a significant reduction in the plasma rf potential in inductive discharges. Note that a purely inductive discharge (unless it is in a non-linear regime [13, 21]) has no rf potential.

3.2. Bulky probes

The apparent simplicity of the Langmuir probe method has promoted the widespread illusion that measurement, processing and interpretation of probe characteristics are commonplace and routine. Indeed, according to Schott [22], 'There is scarcely another procedure of plasma diagnostics involving so many dangers of incorrect measurement and erroneous interpretation of its results than the probe method.' Although, significant progress in refining the probe technique and its application to rf plasmas has been achieved in the recent decade [23–31], the neglect of basic requirements and precautions in making probe measurement is apparent in many probe works. This is especially true when using the Druyvesteyn formula to evaluate the EEDFs in high-density plasmas as found in ICPs. Analysis of problems encountered in probe measurements, specifics of probe diagnostics in rf plasma and some remedies to avoid these problems have been reviewed in our works [24, 25] and in the literature cited therein.

In spite of prevailing lore, the probe method is a non-intrusive plasma diagnostic method when properly used within the assumptions and limitations of its applicability. In essence, probe diagnostic theory (and measurements) accounts for local plasma perturbation caused by the probe, thus coupling local probe perturbation in the probe sheath with unperturbed plasma parameters in the probe's vicinity. This implies that a probe should be small enough not to incur perturbations that are unaccounted for by probe theory.

The well-known requirements of the Langmuir probe method and validity of the Druyvesteyn formula are assumptions of a small probe and a collisionless probe sheath. For a cylindrical probe used in common practice this means: $a[\ln(l/2a)] \ll \lambda_e$, and $\lambda_D \ll \lambda_e$, where a is the probe radius, l is its length, λ_e is the electron mean free path and λ_D is the electron Debye length. The desire to clearly obtain saturation in the ion and/or the electron part of the probe characteristic (to make it look as in textbooks) seems to be the reason for using excessively large probes. Indeed, a properly designed small cylindrical probe at moderate plasma density does not produce a clear saturation in the probe electron current beyond the plasma potential, nor does it show a distinct break at the plasma potential in a semi-log representation of the probe characteristic. The only reliable way to find the plasma potential for such probes is differentiation of the probe characteristic or the use of a small emissive probe [23].

The limitations defined above should be applied not only to the probe tip itself, but also to the whole probe holder immersed in the plasma to avoid a local, and sometimes, a global plasma perturbation. Bulky probe holders are typical for many 'homemade' probes and are common for all known commercial Langmuir probes. Even at very low gas pressure, they present a large recombination surface (similar to a discharge chamber wall) affecting the plasma ionization balance and resulting in depletion of the plasma density near the probe. The 'worst case scenario' known to the authors is insertion of a 1 cm diameter commercial probe holder into a 2.5 cm discharge gap in the GEC reference cell.

In typical high-density plasma, the probe holder (as well as the probe tip) can reach a very high temperature [32] (and can even become red) due to electron and ion bombardment. At such high temperatures, extensive out gassing may occur from the probe holder surface leading to plasma contamination that is proportional to the surface of the probe holder.

3.3. Low frequency noise and drift

The problems of rf noise interfering with probe measurement in an rf plasma are well understood. They are adequately addressed in many ICP experiments by incorporating rf blocking filters tuned to the fundamental frequency and one or more higher harmonics. It has been found empirically that negligible distortion in EEDF measurements [33] occurs in an rf compensated probe when the relation: $V_{rf} \leqslant 0.3T_e/e$ is fulfilled, where V_{rf} is the rms value of the rf component of the probe sheath voltage and T_e is the electron temperature expressed in electronvolt. To satisfy this condition, the probe filter impedance for each rf harmonics Z_f should be such that: $Z_f \geqslant 3eZ_p\Phi_p/T_e$, where Φ_p is the rf plasma potential referenced to ground.

A potential problem of probe diagnostics specific to inductive plasma is rf voltage induced on the probe holder by the induction coil when the induced rf field has a component along the probe holder. This gives rise to an rf potential on the probe tip with respect to ground even in a well screened ICP with no practical rf plasma potential. To avoid this problem, the probe holder should be oriented normal to the induced rf electric field.

Similar to rf plasma potential, low frequency noise and slow drift in the plasma potential can also distort the measured probe characteristic. These relatively slow variations of plasma potential originate from low frequency plasma instability and by ripples and drifts in the rf power source due to the intrinsic capacitive coupling in an ICP. Slow plasma potential variations during probe measurements convolutes the probe I/V characteristic and, due to error magnification inherent to the differentiation procedure, this results in significant distortion in the low energy part of the measured EEDF [25]. To our knowledge, low frequency noise and drift are rarely addressed adequately in EEDF measurements in dc and rf plasmas.

3.4. Probe surface contamination

Distortion of the probe characteristic may also be due to a change in the work-function of probe surface and in probe surface resistance during the probe voltage scan. Under

conditions of changing probe surface resistance and work-function, the probe sheath voltage does not correspond to the applied probe voltage (see [24, 25] and references therein). The probe work-function can vary up to 1 V or more due to a change in probe surface temperature during the probe scan. Surface temperature can change due to changes in probe heating caused by electron current collection. This effect is more pronounced in high-density and chemically active plasmas.

When the probe scanning time T is comparable to the probe thermal equilibrium time τ (usually around 1 s), a hysteresis in the probe I/V characteristic can be seen. There is no hysteresis for $T \gg \tau$ (the common way of probe measurement) and for $T \ll \tau$. In the first case, the probe temperature is in equilibrium with the probe voltage and the probe I/V characteristic is generally reproducible yet distorted, while in the second case, when probe temperature and probe work-function remain constant, the probe I/V is unaffected by the probe work-function. Fast probe scanning times, in the range of milliseconds or less, avoid the convolution effect caused by a change in the probe temperature [24, 25].

A fast probe scan avoids probe overheating and melting when a large electron current is collected in a high plasma density typical of ICP and helicon plasma. The threat of probe melting at high plasma density frequently leads to the use of probe diagnostics based on the ion part of the probe characteristic (which are notoriously unreliable). However, with a fast probe scan it is possible to obtain high quality EEDF measurements at a plasma density as high as 10^{13} cm^{-3} [34]. Also, fast probe scans allow acquisition of a large number of probe characteristics (sufficient for their effective averaging, thus, for reduction of random noise) in seconds. This significantly reduces the effect of discharge drift on the quality of the probe measurement.

Probe surface resistance may pose a problem even in noble gas discharges; probe biasing with negative voltage (30–50 V) for only a few minutes is usually enough to clean the probe (without sputtering) and to keep it clean throughout the measurement. This can be achieved by fast (mS) probe scans combined with a negative or positive probe bias (to keep the probe hot) between probe sweep pulses.

3.5. Probe circuit resistance

Analysis of published EEDF measurements in ICP and other high-density plasma sources shows that probe circuit resistance is the most frequent source of distortion in the measured EEDF. This distortion is due to uncontrolled voltage drop across different elements of the probe current circuit, resulting in a reduction of voltage across the probe sheath [24, 25]. The voltage reduction is: $\Delta V = I_p R_c$, where I_p is the probe current and R_c is the total circuit resistance. The circuit resistance R_c is sum of the probe driver output resistance R_i, the resistance of the probe wires R_w, the contact resistance R_t, the sensor resistor R_v, the resistance of rf filters R_f, and (perhaps the most important part) the sheath resistance near the chamber wall R_s and the surface resistance of the discharge chamber, covered with a low-conductivity layer of plasma reaction products, R_x. Some of these resistances (like R_w, R_t, R_v and R_f) are constant during the probe scan and can be accounted for in processing the probe characteristic. Others (like R_i, R_s and R_x) are unknown, sometimes non-linear (thus, probe current dependent) and are generally not easy to evaluate and account for.

Probe circuit resistance has a major effect on the probe I/V characteristic near the plasma potential where the probe current and thus ΔV are maximal. Due to error magnification inherent in the differentiation procedure, even a relatively small distortion in I/V probe characteristic results in an enormous distortion in the inferred EEDF [24, 25]. This distortion manifests itself in a flattening of the second derivative of the probe I/V characteristic d^2I_p/dV^2 near the plasma potential and in an enlargement of the voltage gap between the second derivative maximum and the zero crossing point. d^2I_p/dV^2 is proportional to the electron energy probability function (EEPF). An EEPF distorted in this way looks like a Druyvesteyn distribution (EEPF $\sim \exp(-\varepsilon^2/a^2)$ (see, for example, figure 4 in [25]). This 'Druyvesteynization' of an EEPF with increasing discharge power and/or gas pressure, can be seen in measurements of many authors and has even been mistaken for a new plasma kinetic effect in ICP.

EEPF depletion due to probe circuit resistance is proportional to $(\Delta V)^3$, [24] and is greatest near the plasma potential, which corresponds to the low energy electrons of the distribution. EEPF distortion depends on the ratio R_{po}/R_c where R_{po} is the minimal probe differential resistance (at plasma potential) $R_{po} = T_e/eI_{eo}$, and I_{eo} is the electron saturation current. As shown in [25], depletion in the second derivative of the probe current (and thus, in the EEPF) by less than 3%, requires the total probe circuit resistance R_c to be smaller than $0.01 \times R_{po}$. That implies that for undistorted EEDF measurements in high-density plasma, typical of an ICP, R_c should be in range between a few milliohms and a fraction of an ohm. This is not easy to achieve in a probe circuit having many resistive components like a filter choke and plasma to chamber wall resistance.

This problem becomes severe in ICP with plasma processing gases, where the metal chamber wall is covered with a low-conductivity layer of the plasma reaction products [10]. Even in argon ICP with clean chamber walls, the wall sheath resistance is frequently comparable to the probe sheath resistance resulting in Druyvesteynization of the measured EEPF. The wall sheath resistance also poses a limit to the maximal gas pressure accessible for probe diagnostics of ICP when the ion current to the chamber wall is less than the electron saturation current to the probe, $n_p S_p (T_e/2\pi m)^{1/2} \geqslant n_w S_w (T_e/M)^{1/2}$, [25], where n_p and n_w are the plasma density at the point of measurement and at the plasma boundary near the chamber wall, S_p, S_w, m, M and T_e are the probe surface, the chamber inner surface, the electron mass, the ion mass, and the electron temperature, respectively.

Saturation of plasma density with increasing gas pressure and/or discharge power, found in some ICP probe measurements, is generally the result of finite probe circuit resistance. This effect is more pronounced at elevated gas pressure when plasma density near the chamber wall is much less than that in the plasma bulk ($n_p \gg n_w$). Note that in diffusion controlled bounded plasmas, $n_w/n_0 \approx \lambda_i/\Lambda$ when $\lambda_i/\Lambda < T_g/T_e$ and $n_w/n_0 \approx (\lambda_i/\Lambda)^{1/2}$ when $\lambda_i/\Lambda > T_g/T_e$, where n_0 is the plasma density in the discharge centre, λ_i is the ion mean free path and T_g is the gas temperature.

The circuit resistance problem remains unsolved in a majority of ICP probe experiments, (as well as in other high-density plasma sources) resulting in a large EEPF distortion in its low energy part. This distortion manifests itself in an enormous depletion (and even, an absence) of low energy electrons in the measured EEPF, while low-energy electrons constitute the majority (up to 90–99%) of the electrons of the distribution. Apparently, the use of large Langmuir probes exacerbates the problem associated with the circuit resistance.

4. Probe experiment design

4.1. Experimental setup

Probe measurements have been carried out in an ICP operated over a wide range of external parameters in a cylindrical stainless steel discharge chamber with a Quartz bottom window as shown in figure 1 and described in detail in [18]. The chamber ID is 19.8 cm, its length is 10.5 cm, and the Quartz thickness is 1.27 cm. A planar induction coil with a 12.7 cm OD and a 3.8 cm ID is mounted 1.9 cm below the bottom surface of the discharge chamber. At high frequency (13.56, 6.78 and 3.39 MHz), the coil consists of five turns. An electrostatic shield and an air gap located between the glass and the coil practically eliminate capacitive coupling of coil voltage into the plasma. For low operating frequency (0.45 and 0.9 MHz), the coil consists of 20 turns of litz wire and there is no need for a electrostatic shield. An aluminium kettle covers the induction coil from below and acts as an rf shield preventing electromagnetic interference on the measurement apparatus and associated wiring. A 7.6 cm window for plasma monitoring is fixed close to the cylindrical chamber surface to minimize distortion of the cylindrical surface of the chamber. Four radially directed NW16 flanges are welded symmetrically on the cylindrical chamber surface in the chamber mid-plane and four similar flanges are welded symmetrically to the top chamber plate at a radius 4 cm from the chamber axis (corresponding to the maximum in the radial distribution of the electromagnetic field). These flanges serve as ports for installation of moveable stages with Langmuir, magnetic and thermal probes. Additionally, three 3.8 cm vacuum ports are fixed on the chamber radial wall having four 0.95 cm holes (forming grids preventing plasma diffusion out of the chamber) inside of the port welding. These ports serve as a gas inlet, a gas outlet and a Baratron® connection.

The discharge chamber is pumped with a 170 l s^{-1} turbo pump backed with a mechanical roughing pump. The ultimate vacuum is in the range of 10^{-7} Torr, which is achieved after baking and cleaning with gas flow at maximal discharge power (∼400 W). A residual gas analyzer is used to monitor residual gas content. We found that without baking and cleaning, the discharge at the mTorr pressure range can be contaminated by gas coming from the chamber wall due to intensive ion bombardment and chamber heating. Gas purity during ICP operation is maintained by gas flow with an automatically regulated gas pressure. The flow rate does not affect the discharge electrical, thermal and plasma characteristics and is between 1 and 20 sccm (depending on working argon pressure). The working gas pressure was measured with two Baratron® heads rated for a maximal gas pressure of 0.1 and 10 Torr.

An automatic control system [18] programmed to control the working gas pressure p and the rf power absorbed by the plasma P_d and to display the ICP and rf system electrical characteristics is routinely used during the plasma probe diagnostics. This system maintains the rf power dissipated in plasma P_d at a programmed level, continuously adjusting elements of rf power system to compensate the effect of their temperature drift on P_d. The discharge power P_d is determined by measuring transmitted power and subtracting matcher and coil losses that were determined *a priori* as a function of coil current and temperature [18]. In what follows all mention of power refers strictly to power dissipated in the plasma P_d.

A detailed data base on the ICP electrical characteristics for rf frequencies: $\omega/2\pi = 3.39$; 6.78 and 13.56 MHz, argon pressures: between 0.3 and 300 mTorr, and discharge powers between 12.5 and 200 W, are reported in [18]. These data include coil voltage and current, the plasma resistance and reactance transformed to the inductor coil, the power transfer efficiency and the rf plasma potential. Additionally, rf magnetic and electric fields and rf current density were measured with two-dimensional magnetic probes and have been published elsewhere [12, 35–38].

4.2. Langmuir probes

Movable Langmuir probes have been constructed for space-resolved measurements along the discharge's axial and radial direction. Probes are mounted on sliding stages fixed on NW-16 flanges, thus allowing for precise linear probe positioning through vacuum Ultratorr® connectors. The Langmuir probe assembly shown in figure 2 is designed to

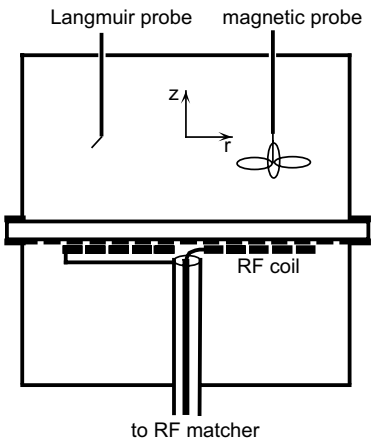

Figure 1. Schematic diagram of experimental ICP chamber with Langmuir and magnetic probes.

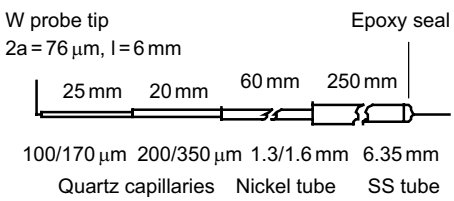

Figure 2. A detailed sketch of an 'L' type Langmuir probe showing the telescoping assembly of quartz capillary tubes and metal tubes.

minimize plasma perturbation and at the same time to be rigid enough to insure stable probe positioning. For these purposes the probe support is a telescoping structure with a progressively smaller diameter nearing the probe tip.

The probe is made of 76 μm tungsten wire (8 cm long) welded to a 0.5 mm nickel wire lead. The probe tip is 6 mm long and is bent 90° with respect to the rest of the probe wire. The probe wire closest to the probe tip is covered with quartz capillary tubing, 100 μm ID and 170 μm OD that is about 25 mm long. Being nearest to the probe tip, this is the most critical section of the probe holder with regard to plasma perturbation; therefore, its diameter is made as small as possible. The first capillary section of the probe holder is inserted into a second one having a 200 μm ID, 350 μm OD and a length of 20–30 mm. The second capillary is fixed to nickel tubing 1.3 mm ID, 1.6 mm OD and 60 mm length, via a gas transparent metal insertion to allow pumping out gas from the probe holder interior. The nickel tubing, in turn, is inserted via a second transparent insertion into the main body of the probe holder made of $\frac{1}{4}$ inch SS tubing having 6.35 mm OD and a length of 175 mm. At the tubing end, the nickel probe lead wire with a ceramic spacer is sealed to the tubing using vacuum epoxy. The last quarter inch section of the probe holder is fixed on the movable stage outside discharge chamber. An Ultratorr® vacuum feed through connector provides vacuum sealing of the probe holder from the atmosphere.

Our experiments [32] with probes immersed in the ICP have shown that even at relatively modest discharge power, thin probes and probe holders acquire a rather high temperature, considerably exceeding the working gas temperature. The temperature of a Quartz capillary 0.4 mm OD, placed in the centre of a 100 W ICP has reached 275°C, 338°C, 532°C and 595°C, for argon pressure 1 mTorr, 10 mTorr, 100 mTorr and 1000 mTorr, respectively. Even higher probe temperatures are attainable at higher discharge power and gas pressure; floating probe tip and Quartz capillary in our experiments became red at elevated gas pressures and discharge powers of 200 and 400 W.

The high probe temperature that occurs in high-density plasma (mainly due to ion bombardment) requires special attention on probe materials and their compatibility when designing a probe experiment. We do not recommend the use of ceramic capillary tubing (found in a majority of published probe experiments) because its wall is too thick, thereby introducing too much plasma perturbation in the vicinity of the probe tip. High probe temperatures found in high-density plasmas cause unavoidable probe out gassing. The larger the probe size, the more intensive the probe outgassing and the more time needed to clean the probe (not only its tip but the entire probe body).

A high probe temperature also results in an increase of probe lead wire resistance (a few times larger than at room temperature). In a 200 W, 100 mTorr ICP, when the plasma density reaches about $4 \times 10^{12}\,\mathrm{cm}^{-3}$, corresponding to a minimal probe sheath resistance $R_{\mathrm{po}} = 7.8\,\Omega$, an 8 cm long, 76 μm diameter tungsten probe lead is estimated to be about 700°C and have a resistance $R_{\mathrm{w}} = 2.8\,\Omega$, $R_{\mathrm{w}}/R_{\mathrm{po}} = 0.36$. This in itself would lead to suppression of the second derivative at the plasma potential and to reduction of low energy electrons in the measured EEDF of about three times. Increasing the discharge power up to 1 kW (typical in many ICP experiments) the estimated probe lead temperature could reach 1000°C, which would increase probe lead resistance R_{w} to about 4.2 Ω, while the minimal probe sheath resistance R_{po} would reduce to 1.6 Ω. As a result, the ratio $R_{\mathrm{w}}/R_{\mathrm{po}} \approx 2.7$, would dramatically reduce the number of low energy electrons in the measured EEDF making a Maxwellian EEDF appear quite similar to Druyvesteyn EEDF.

Probe diagnostics in high-density plasma have the advantage of continuous probe cleaning by intensive flux of plasma electrons and ions coming to the (floating) probe surfaces. This eliminates the need for biasing the probe with high negative (for ion bombardment) or positive (for electronic heating) voltage. Probe surface cleaning (usually accompanied with outgassing) takes about an hour at maximal discharge power at a gas pressure (about 100 mTorr) sufficient to provide enough plasma density.

4.3. Probe measurement and processing

Accurate measurement of the volt/ampere characteristic of the probe sheath in gas discharge plasma is not a trivial task. As a rule, the probe current and voltage measured directly at some point of the probe circuit is not identical to the current and voltage across the probe sheath. As mentioned earlier, a variety of stray resistances are distributed over the entire probe circuit and the assumption that all of them are negligible is quite illusive.

A schematic diagram of Langmuir probe measurement in a plasma contained in a grounded metal chamber (or in contact with a large electrode) is shown in figure 3(*a*), together with its corresponding equivalent circuit (figure 3(*b*)). The probe current I_{p} flows from the grounded probe voltage source (PVS) back to ground through various parts of the probe circuit: the external resistance R_{ext}, which includes all resistances located between the probe tip and the PVS, $R_{\mathrm{ext}} = R_{\mathrm{w}} + R_{\mathrm{t}} + R_{\mathrm{v}} + R_{\mathrm{f}}$, the probe sheath resistance R_{psh} and the internal resistance R_{int} consisting of the chamber sheath resistance R_{s}, the chamber surface resistance R_{x} and the plasma R_{pl} resistance, $R_{\mathrm{int}} = R_{\mathrm{s}} + R_{\mathrm{x}} + R_{\mathrm{pl}}$. The source of plasma potential (generally containing dc, rf and low frequency components) is shown in the equivalent circuit as a residual (noise) voltage source (RVS). Here, we assume that rf plasma potential is adequately addressed, that the probe is clean enough to neglect

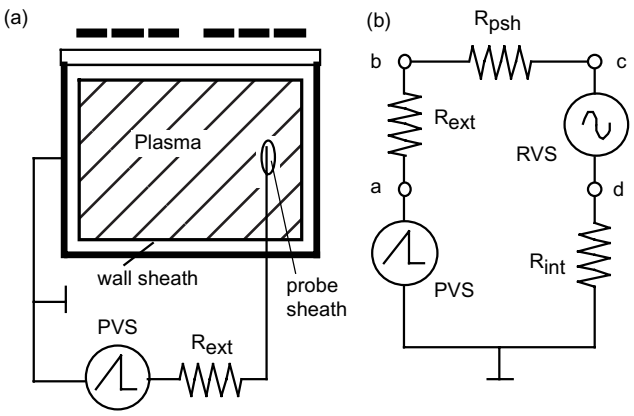

Figure 3. Schematic diagrams of: (*a*) grounded wall ICP with Langmuir probe, (*b*) electrical equivalent circuit.

probe surface resistance and that the plasma resistance R_{pl} is negligibly small, $R_{pl}/R_{po} \approx (a/\lambda_e)\ln(l/2a) \ll 1$.

In practice, the probe voltage referenced to ground V_a is measured at the point represented as 'a' in figure 3(*b*). Therefore, it includes not only the voltage drop across the probe sheath V_p, but also the voltage drops across the external resistor $V_{ext} = I_p R_{ext}$ (for example, due to resistance of the probe wire and the rf filter), the voltage across the internal resistance $V_{int} = I_p R_{int}$ and the residual voltage V_r, ($V_a = V_p + V_{ext} + V_{int} + V_r$). In order to infer the true voltage across the probe sheath V_p one has to account for stray voltages V_{ext}, V_{int} and V_r.

Different approaches (for different parts of the circuit) are used in our probe experiment to address the circuit resistance issue [25]. The residual voltage V_r and the voltage drop across the internal resistance V_{int} (i.e. the instantaneous value of plasma potential) are cancelled by an active electronic circuit by measuring the plasma potential (at the point *c* in figure 3(*b*)) with an additional reference probe RP and introducing the potential to the measuring circuit with the measurement probe (MP) in the opposite phase, as shown in figure 4. This procedure cancels, not only the voltage drop across the internal resistance, but also any dc voltage and low frequency noise originated in the plasma and in the chamber wall sheath, providing that frequency and phase bandwidth of the electronic probe circuit overlaps the spectrum of probe and noise signals.

The compensation of the voltage drop across the external resistance (and reactance) is achieved by arranging the negative output impedance of the probe driving circuit to be equal and opposite to the impedance of the external part of the probe circuit. Reactance compensation is needed when using a fast probe voltage sweep together with rf resonant filters whose inductive reactance cannot be neglected for high frequency components of the probe current.

The probe driving circuit shown in figure 4 includes a variable sensor resistor R_v fed to a differential amplifier. The circuit is able to generate a fast (between a fraction and a few mS) sweep of the probe voltage with up to 1 A probe current drive and produces an output voltage proportional to the probe current. The driving circuit has an analog bandwidth of few hundred kilohertz and is able to effectively compensate stray voltage drops across different parts of the probe circuit and to suppress low frequency noise in the plasma potential.

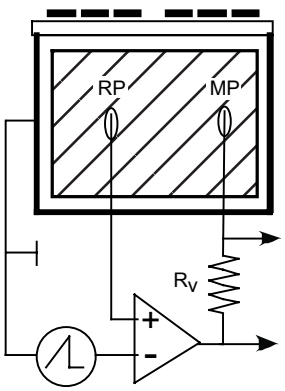

Figure 4. Conceptual diagram of a circuit for cancelling the residual voltage and the voltage drop across the internal resistance, as well as to compensate for dc and low frequency noise voltage. RP is the reference probe and MP is the measuring probe.

The circuit does not compensate the time variation in the probe current due to plasma density and electron temperature (or EEDF) oscillations, and therefore, it can be used in a time resolved mode with appropriate signal acquisition and processing. On the other hand, measurement in strongly unstable plasma, with a standard acquisition and processing with ensemble averaging, could be considerably convoluted in the process of ensemble averaging of probe characteristics when trying to improve the signal-to-noise ratio. A detailed description of the function of this circuit is given elsewhere [25].

The output voltage proportional to the probe current I_p is acquired by a PC using a 12 bit DAQ card that ensemble averages 500–1000 probe I/V characteristic followed by digital double differentiation and adaptive filtering. The electron probability function $f(\varepsilon)$ found from the second derivative of the probe characteristic d^2I_p/dV^2 is used to calculate plasma parameters n and T_e, electron–atom ν_{en}, electron–electron ν_{ee} and electron–ion ν_{ei} collision frequencies, as well as, ionization ν_i and excitation ν^* frequencies. Acquisition, processing and display of the calculated function $f(\varepsilon)$, the plasma parameters and the rates of gas discharge processes takes about 10 s. Since the rf plasma potential Φ_{rf} measured in this ICP is relatively small ($\Phi_{rf} \ll T_e$) no rf filter was used in the EEDF measurement.

5. Experimental results and discussion

Measurements were made with a number of driving frequencies $\omega/2\pi = 13.56$, 6.78, 3.39, 0.90 and 0.45 MHz in argon discharges at fixed gas pressures of 1, 10 and 100 mTorr and at fixed rf power dissipated in plasma of 12.5, 25, 50, 100 and 200 W. Some preliminary results obtained in this ICP arrangement have been highlighted elsewhere [6, 7, 12, 13, 14]. Here, we report on electron probability function and plasma parameters measured in the ICP centre, mostly with a fixed driving frequency of 6.78 MHz. Spatial variation of $f(\varepsilon)$ and plasma parameters will be published elsewhere.

The range of discharge power was limited at the low end by stability of the discharge while the upper end was limited by the available rf power source (ENI A-500 RF Amplifier) and by a desire to avoid excessive probe overheating in high-density plasma. The range of argon pressure was limited at the low end by the condition of stable ionization balance at all levels of discharge power, while the upper end of argon pressure was limited by the ion saturation current to the chamber wall that is equal to the maximal electron current to the probe, when plasma density on the plasma boundary is much smaller than that in the plasma centre where probe measurement were performed.

5.1. Electron energy probability function

The electron energy distribution is represented in this paper in terms of the EEPF, $f(\varepsilon)$, that is proportional to the measured second derivative of the probe characteristic, d^2I_p/dv^2. $f(\varepsilon) = 2(2m)^{1/2}(S_p e^3)^{-1} d^2I_p/dV^2$ is related to the EEDF, $F(\varepsilon)$, as: $F(\varepsilon) = \varepsilon^{1/2} f(\varepsilon)$. No account is made for the contribution of the ion component to the second derivative of the probe characteristic (d^2I_i/dV^2), since in the electron

energy range presented in our experiment the contribution of $d^2 I_i/dV^2$ to the total second derivative is negligibly small [24–26].

The electron probability function measured in the ICP centre ($z = 5.2$ cm, $r = 0$) at fixed driving frequency of 6.78 MHz and different ICP absorbed power, are shown in figures 5–7, for 100 mTorr, 10 mTorr and 1 mTorr, respectively. EEPFs are graphed in a semi-log plot to display them over a wide dynamic range and to show at a glance their deviation from a Maxwellian EEPF, which in this representation is a straight line. EEPFs in figures 5–7 are given in a sequence of doubling rf power with the smallest and the largest powers noted.

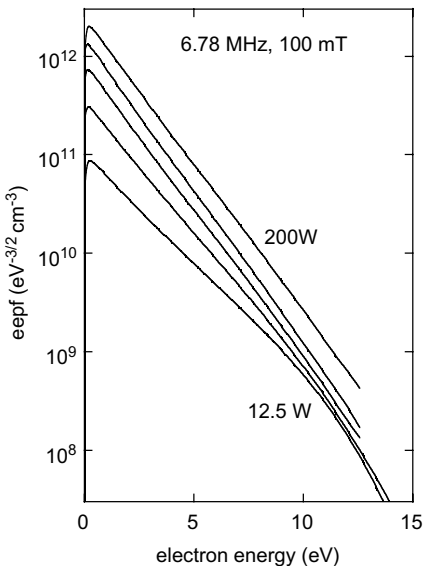

Figure 5. The EEPF versus electron energy for 12.5, 25, 50, 100 and 200 W for a driving frequency $\omega/2\pi = 6.78$ MHz and a gas pressure of 100 mTorr.

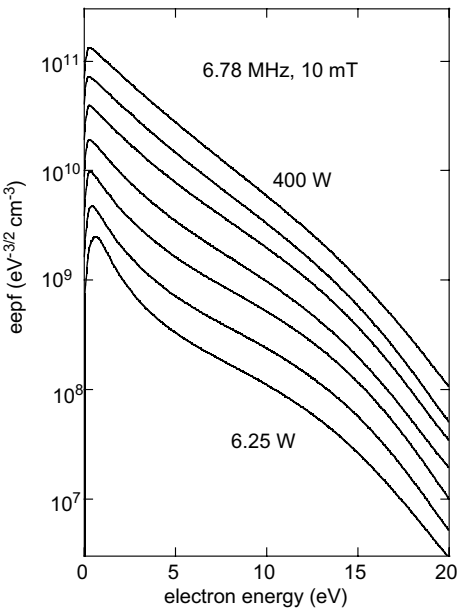

Figure 6. The EEPF versus electron energy for 6.25, 12.5, 25, 50, 100, 200 and 400 W for a driving frequency of 6.78 MHz and a gas pressure of 10 mTorr.

At an argon pressure of 100 mTorr (figure 5) the ICP is collisionally dominated and controlled by ambipolar diffusion, $T_g/T_e > \lambda_i/\Lambda \ll 1$, ($\lambda_i \approx 3 \times 10^{-2}$ cm $\ll \Lambda \approx 4$ cm) and plasma impedance is unaffected by electron thermal motion ($v_{th}/\delta < (\omega^2 + \nu_{en}^2)^{1/2}$), [7, 39, 40] where v_{th} is the electron thermal velocity, $v_{th} = (2T_e/m)^{1/2}$ and δ is the skin depth. Under such conditions the ICP operates in the domain of normal skin effect (local regime), where discharge current density J is locally coupled with the rf electric field E through the cold plasma conductivity formula, $J = \sigma_p E$.

For all discharge powers, the EEPFs shown in figure 5 are very close to a Maxwellian distribution in the elastic energy range ($\varepsilon < \varepsilon^*$) and are depleted in the high-energy inelastic energy range ($\varepsilon > \varepsilon^*$), where ε^* is the excitation energy for argon (11.55 eV). The electron temperature (which is inversely proportional to the EEPF slope in semi-log scale) is falling with discharge power while the energy interval where the EEPF remains Maxwellian is growing. These trends in EEPF behaviour are typical for high-density discharge plasma (independent of the specific electron heating mechanism in the discharge maintaining electric field, i.e. for dc, rf or microwave discharges). At high plasma density, electron–electron collisions (whose frequency $v_{ee} \propto n\varepsilon^{3/2}$) 'Maxwellianize' the low energy part of EEPF, while two-step processes via atomic excited states mainly control ionization leading to a growth in the ionization frequency and a reduction of electron temperature with plasma density.

EEPFs, measured over a wide range of discharge power at 10 mTorr are shown in figure 6. For this argon pressure, where $T_g/T_e < \lambda_i/\Lambda \ll 1$, plasma diffusion to the chamber wall and to the window is controlled by ion charge exchange collisions [41, 42], while the quantities v_{th}/δ, ω and ν_{en} are comparable [35, 43], thus defining a weakly non-local ICP regime (slight anomalous skin effect) where electron collisional and thermal (stochastic) effects are comparable.

The EEPF at 10 mTorr and at low discharge power is a three-temperature structure with a well-expressed low energy bump and a fall in the inelastic energy range. At this pressure,

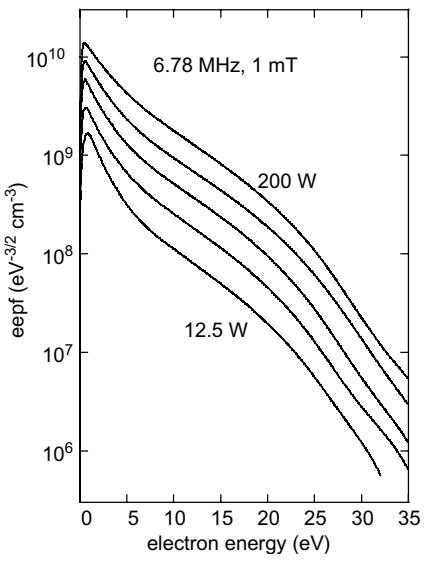

Figure 7. The EEPF versus electron energy for 12.5, 25, 50, 100, and 200 W for a driving frequency of 6.78 MHz and a gas pressure of 1 mTorr.

direct and two-step ionization processes take place; the first prevails at low discharge power (plasma density) and the second prevails at high discharge power. The EEPF in the elastic energy range evolves into a Maxwellian distribution with increasing discharge power due to enhancement in electron–electron collisions leading to equalization of the distribution temperature $T_{ed} = -[d \ln f(\varepsilon)/d\varepsilon]^{-1}$ of low and middle energy electron groups.

The EEPF at 10 mTorr and low discharge power has a structure similar to that found in capacitive coupled plasma (CCP) [44]. Although rf field directions in these discharges are different, EEPF similarity in CCP and ICP is due to similarity in rf heating and dc ambipolar field profiles in both type of discharges. The appearance of a low energy peak in the EEPF is a natural consequence of non-local electron kinetics [45–47] in low-pressure rf discharges at moderate plasma density (capacitive, inductive or wave driven) where rf power absorption is localized along the plasma boundary (in rf sheath and/or skin layer). Due to the ambipolar dc potential inherent to bounded plasma, low energy electrons are trapped by the ambipolar potential well into the plasma bulk, thus they are prevented from participating in the heating process at the plasma boundary (in the skin layer or the rf sheath). Therefore, mainly the electrons of the middle energy group are able to participate in the heating process. As for the EEPF tail of energetic electrons corresponding to inelastic energy range ($\varepsilon > \varepsilon^*$), their contribution to total electron heating is also negligible due to their small population, their escape to the wall and their ineffective collisionless interaction with the rf field in the skin layer.

EEPFs for 1 mTorr are shown in figure 7. At this gas pressure, plasma loss to the wall is controlled by ion inertia and the discharge is close to the ion-free path (Tonks–Langmuir) regime ($\lambda_i \approx \Lambda$, $\lambda_e \gg \Lambda$), while electron interaction with the electromagnetic field is strongly affected by electron thermal motion. This is the domain of anomalous skin effect ($\upsilon_{th}/\delta > (\omega^2 + \nu_{en}^2)^{1/2}$) [48] with non-monotonic electromagnetic field and rf current distributions and non-collision power absorption [7, 36, 40, 49] typically found. The three-temperature structure in the EEPFs is more expressed here than at 10 mTorr and is observed over the entire power range since (at similar discharge power) the plasma density is lower and the electron temperature is higher than at 10 mTorr. Recall that the electron–electron collisions responsible for Maxwellization are proportional to $n\varepsilon^{3/2}$. The change in the EEPF slope in the inelastic energy range is shifted to electron energy higher than excitation, ε^* and ionization, ε_i energy and is close to the plasma potential ($V_p = 24$–25 V) referenced to the grounded chamber because fast electron escape to the wall is the main electron energy loss process in this discharge regime.

The EEPF measured in the discharge centre at different argon pressure and fixed discharge power of 12.5, 50 and 200 W are shown in figures 8–10. These are the same data as in figures 5–7 but the EEPFs are presented so as to exhibit pressure effects at a fixed rf power. At 100 mTorr at the lowest rf power of 12.5 W (figure 8) electron–electron collisions can Maxwellize only relatively low energy electrons (with energy less than 10 eV) thus a significant part of the EEPF in inelastic energy range is depleted. At higher discharge power, the energy range for Maxwelization becomes larger and the limited

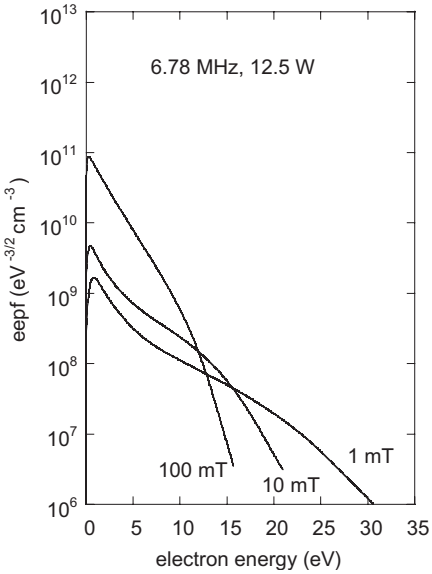

Figure 8. The EEPF versus electron energy for 1, 10 and 100 mTorr in a 12.5 W discharge driven at 6.78 MHz.

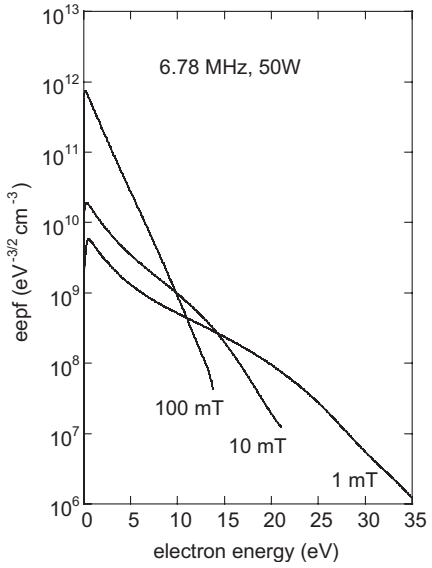

Figure 9. The EEPF versus electron energy for 1, 10 and 100 mTorr in a 50 W discharge driven at 6.78 MHz.

dynamic resolution of EEPF measurement (about four orders of magnitude) hinders detection of depletion in the high-energy tail of the EEPF.

The EEPFs in figures 5–10 differ significantly from those found in the literature, mainly in their low energy part where a majority authors have measured EEPFs with significant deviation from Maxwellian distribution, resembling a Druyvesteyn distribution. This departure from a Maxwellian distribution growing with discharge power and with gas pressure (and therefore with plasma density) appears to contradict the well-established role of electron–electron collisions leading to EEPF Maxwellization. As discussed above, the reason for distortion in the EEPFs measured at elevated power and pressure is too large probe circuit resistance whose effect increases with plasma density.

5.2. Basic plasma parameters

The basic discharge parameters: the plasma potential, the plasma density and the electron temperature are given in figures 11–13, respectively. The plasma potential V_p shown in figure 11 is the probe potential referenced to the grounded metal chamber at the zero crossing point of the second derivative d^2I_p/dV^2. Due to the absence of a substantial rf plasma potential in our ICP, the dc plasma potential is not distorted by the sheath rectification effect and $V_p = V_{sh} + V_a$. In this case, V_p mainly consists of the voltage drop across the chamber wall sheath V_{sh} (floating potential) and the ambipolar voltage V_a between the plasma centre and the plasma edge (i.e. relatively small). Only at relatively high gas pressure when the edge plasma density is much smaller than that in the centre does V_a becomes comparable to V_{sh}.

Both V_a and V_{sh} are defined by the electron temperature. Their dependence on discharge power is similar to $T_e(P_d)$ but they are governed by the different parts of the electron energy distribution. For a Maxwellian plasma, $V_a = (T_e/e)\ln(n/n_s)$, while sheath voltage is defined by the balance between the Bohm flux of ion current to the chamber wall and the current of fast electrons able to overcome the wall sheath, $V_{sh} = (T_e/2e)\ln(M/2\pi m)$, where n and n_s are the plasma density in the plasma centre and the plasma edge, respectively. For a non-Maxwellian plasma, the quantities V_a and V_{sh} can be found as integrals of the EEDF [45, 47]. Generally, the plasma ambipolar potential, the ion current to the wall and the Debye length are defined by so-called electron screening temperature T_{es} which is weighted by the low energy part of the EEPF, while the current of fast electrons to the wall is governed by the tail of the EEPF [26, 50]. For a Maxwellian distribution, $T_{es} = T_e$, for a convex (Druyvesteyn-like) distribution $T_{es} > T_e$ and for a concave distribution (similar to those in figures 6 and 7) $T_{es} < T_e$, where T_e is the effective electron temperature defined by the mean electron energy $\langle\varepsilon\rangle$, ($T_e = 2/3\langle\varepsilon\rangle$).

The power dependence of the effective electron temperature T_e, the screening electron temperature T_{es} and the plasma density n are given in figures 12 and 13 for 1, 10 and 100 mTorr. T_e, T_{es} and n are calculated using the measured EEPF, $f(\varepsilon)$, in accordance with the formulae:

$$T_e = \frac{2}{3}\langle\varepsilon\rangle = \frac{2}{3n}\int_0^\infty \varepsilon^{3/2} f(\varepsilon)\,d\varepsilon$$

$$T_{es} = \frac{2}{n}\left(\int_0^\infty \varepsilon^{-1/2} f(\varepsilon)\,d\varepsilon\right)^{-1}$$

$$n = \int_0^\infty \varepsilon^{1/2} f(\varepsilon)\,d\varepsilon$$

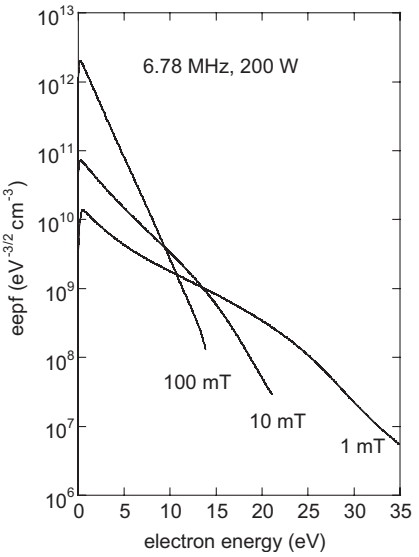

Figure 10. The EEPF versus electron energy for 1, 10 and 100 mTorr in a 200 W discharge driven at 6.78 MHz.

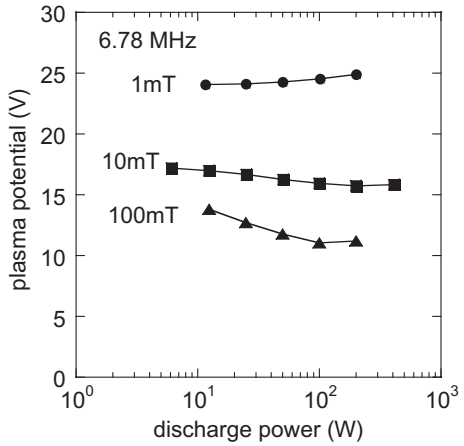

Figure 11. Plasma potential versus discharge power for gas pressures of 1, 10 and 100 mTorr.

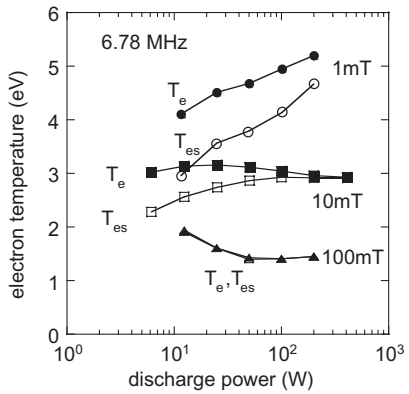

Figure 12. The electron screening temperature and the effective electron temperature versus discharge power for gas pressures of 1, 10 and 100 mTorr.

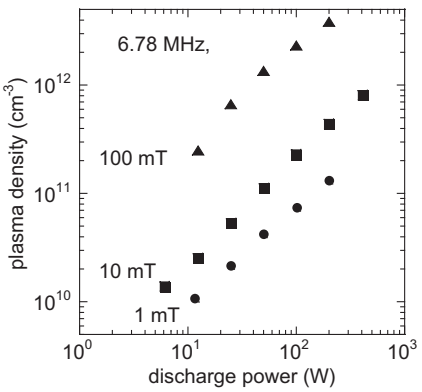

Figure 13. Plasma density versus discharge power for gas pressures of 1, 10 and 100 mTorr.

In these calculations, the EEPF was exponentially extrapolated to zero energy. Due to the very small energy gap between zero and the maximum of the measured second derivative of the probe current, the difference in EEPF integrals calculated with and without extrapolation was less than a few per cent.

Figure 12 shows that T_e and T_{es} coincide over the entire power range at an argon pressure of 100 mTorr. T_e and T_{es} are practically equal because their corresponding EEPFs are mainly Maxwellian over a large dynamic range (over four orders of magnitude). The fall in electron temperature with discharge power is typical for gas discharges at this pressure and is a consequence of two-step ionization, which with increasing electron density requires a lower electron temperature to provide the required ionization rate. The electron temperature in this collisionally dominated ICP is similar to that in a dc positive column of an argon discharge with a similar $p\Lambda$ product and discharge current density.

The values of T_e and T_{es} at low argon pressure (1 and 10 mTorr at low discharge power) differ from each other but both generally increase with discharge power. This is quite opposite to the normal trend usually observed in gas discharge plasma (as at 100 mTorr). The unusual electron temperature dependence is due to an excess of low energy electrons in the electron energy distribution that reduces the effective (averaged) electron temperature. This excess of low energy electrons disappears with an increase in discharge power due to electron–electron collisions, thus resulting in the elevation of the effective electron temperature at higher electron density.

At moderate argon pressure (10 mTorr) and low discharge power, the heating of low energy electrons by high-energy electrons via electron–electron collisions [50, 51] results in both electron temperatures growing with power. At larger discharge power, the electron temperature drop due to two-step ionization prevails, the EEPF becomes close to Maxwellian and T_{es} approaches T_e.

The plasma density dependence on discharge power in the centre of the discharge is shown in figure 13 for different gas pressures. As is common for gas discharges, the plasma density is nearly proportional to the discharge power with that trend slowing down at large discharge power due to gas heating. The measured values of plasma density at the discharge centre shown in figure 13 are somewhat higher that those measured by others authors under similar conditions. We believe there are two main reasons for this. The first is the characterization of our ICP by the rf power dissipated in plasma rather than by rf power delivered to the ICP system (which is always larger and often much larger than that dissipated in plasma). The second reason is an adequate handling of the probe circuit resistance in our probe measurement system avoiding suppression of the low energy part of the EEPF.

Having measured plasma density and electron temperature one can evaluate the gas temperature in the chamber centre. Gas heating is due to electron–atom elastic collisions and ion–atom charge exchange during ambipolar plasma flow to the chamber wall. The first mechanism dominates at high gas pressure while the second mechanism dominates at low gas pressure. The gas temperature in the centre of the discharge has been calculated based on the measured electron density and the effective electron temperature. This calculation assumes

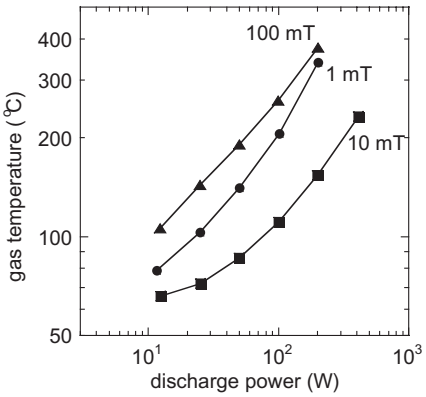

Figure 14. Calculated gas temperature in the centre of the discharge versus discharge power for a gas pressure of 1, 10 and 100 mTorr.

a one-dimensional model of plasma slab with thickness of 2Λ, a parabolic plasma density distribution and a Maxwellian EEPF [32].

The ratio of ion heating rate to electron heating rate is estimated as [32]:

$$\frac{P_i}{P_e} \approx \left(\frac{M}{m}\right)^{1/2} \lambda_e \lambda_i^{1/2} \Lambda^{-2/3} \propto (p\Lambda)^{-2/3}$$

The argon temperature calculated at the chamber centre as function of the discharge power is shown in figure 14. One can see that even at a relatively modest discharge power of 200 W, the absolute gas temperature in the chamber centre is about twice the room temperature resulting in two-time reduction in the gas density there.

5.3. Calculation of characteristic frequencies

It is well-known that an assumption of a Maxwellian electron energy distribution can lead to enormous error in calculating plasma-chemical reaction rates like excitation and ionization. Moreover, due to the dependence of electron–atom collision frequency on electron energy $(d\nu_c/d\varepsilon) \neq 0$, transport coefficients for plasma electrons are also sensitive to EEDF shape, especially for Ramsauer gases like argon, krypton and xenon. Relations coupling the plasma conductivity, its Ohmic (real) and its reactive (imaginary) parts and the rates of inelastic processes with basic plasma parameters are needed for any kind of global and fluid ICP model, or, for just a rough estimate of ICP electrical and plasma parameters.

The plasma electrical conductivity for cold plasma σ_p expresses the relation between the local current density J and the local electric field E through Ohm's law, $\sigma_p = J/E = ne^2/m(\nu_{en} + j\omega_{eff})$, where ν_{en} is the electron transport collision frequency in rf field, and ω_{eff} is the effective rf field frequency. Generally, $\omega_{eff} \neq \omega$ and ν_{en} is not equal to the electron-neutral collision frequency ν_c averaged over electron velocity distribution, $\nu_{en} \neq \langle \nu_c \rangle = \langle Nvs \rangle$, where N, v and s correspond to the gas density, the electron velocity and electron-neutral transport cross-section. The values of ν_{en} and ω_{eff} are defined by equating the given above expression for plasma conductivity to that given by kinetic theory [52],

$$\sigma_p = -\frac{2ne^2}{3m} \int_0^\infty \frac{\varepsilon^{3/2}}{\nu_c(\varepsilon) + j\omega} \frac{df_e}{d\varepsilon} d\varepsilon$$

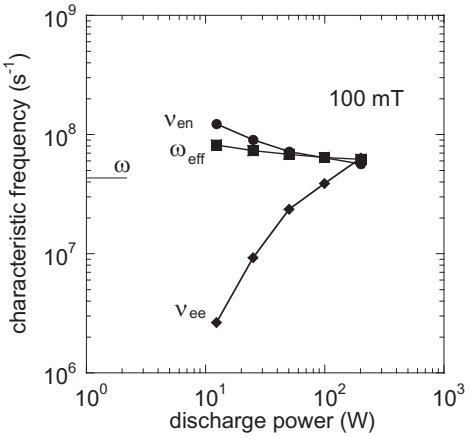

Figure 15. Characteristic frequencies: ν_{en}, ω_{eff} and ν_{ee} versus discharge power in an ICP with a gas pressure of 100 mTorr. ω is the driving frequency.

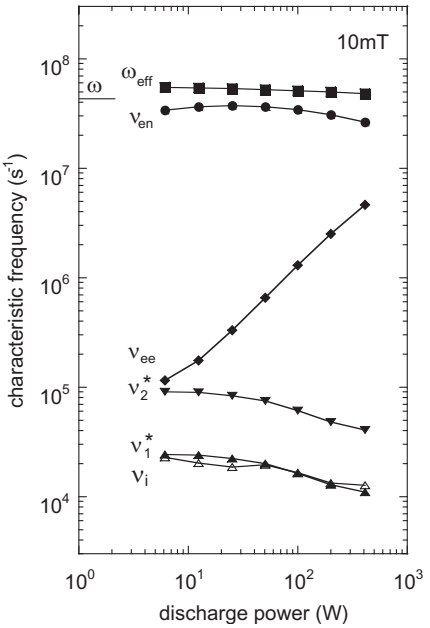

Figure 16. Characteristic frequencies: ν_{en}, ω_{eff}, ν_{ee}, ν_2^*, ν_1^* and ν_i versus discharge power in an ICP with a gas pressure of 10 mTorr.

The calculated values of ν_{en}, ω_{eff} together with the frequency of direct ionization ν_i, the excitation frequency ν^* and the electron–electron collision frequency ν_{ee} are given in figures 15–17 as functions of the discharge power, correspondingly, for 100, 10 and 1 mTorr. The quantities ν_i and ν^* are calculated using the EEPF measured in the experiment and corresponding cross-sections for direct ionization and excitation.

The electron–electron collision frequency ν_{ee} is calculated using the conventional formula [53] (derived for a Maxwellian electron distribution) using the electron screening temperature T_{es} found as an integral of experimental EEPF, $\nu_{ee} = 2.9 \times 10^{-6} n \ln \Lambda_C / T_{es}^{3/2}$, where $\ln \Lambda_C$ is the Coulomb logarithm. The absence of a corresponding formula for ν_{ee} with arbitrary electron energy distribution and the fact that ν_{ee} (similarly to T_{es}) is mainly governed by low energy electrons are the reasons for using T_{es} in determining ν_{ee}.

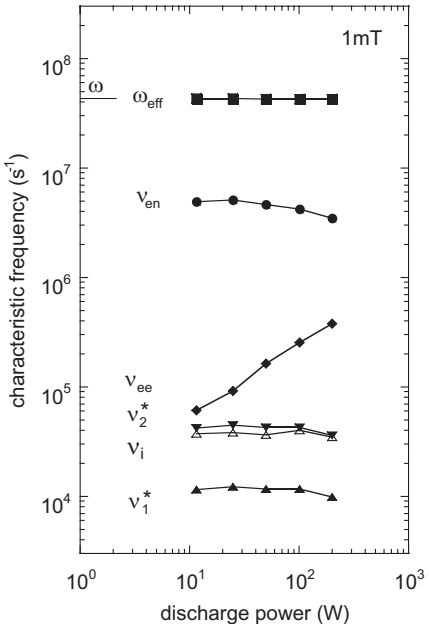

Figure 17. Characteristic frequencies: ν_{en}, ω_{eff}, ν_{ee}, ν_2^*, ν_1^* and ν_i versus discharge power in an ICP with a gas pressure of 1 mTorr.

The dependencies of the characteristic frequencies ν_{en}, ω_{eff} and ν_{ee} on discharge power for 100 mTorr are shown in figure 15. The limited electron energy range where the EEPF can be reliably measured precludes calculation of ionization and excitation frequencies for this gas pressure. Note that ω_{eff} is 1.5–2 times larger than ω, while ν_{en} changes by a factor of three in the rf power range between 12.5 and 200 W. The electron–atom collision contribution to the plasma reactance in this case is comparable to that due to electron inertia (proportional to ω). The changes in electron temperature at low discharge power (see figure 12) and gas heating at high discharge power (leading to saturation in the plasma density, see figure 13) result in a significant change of ν_{en} and in the non-linear dependence of ν_{ee} on discharge power as shown in figure 15.

Due to the large plasma density and the relatively small electron temperature, the values of ν_{en} and ν_{ee} are comparable at 100 mTorr in an ICP with discharge power of 200 W. Plasma conductivity at this and higher power (plasma density) is affected by both, electron–ion ν_{ei} and electron–electron ν_{ee} collisions [53]. At higher plasma density, when Coulomb collisions are more frequent than electron–atom collisions ($\nu_{ee} \approx \nu_{ei} \gg \nu_{en}$), plasma conductivity is defined by the corresponding expression for fully ionized plasma [53]. Note that when ν_{en} and ν_{ei} are comparable the resulting effective transport electron collision frequency is not equal to sum of ν_{en}, ν_{ei} and a part of ν_{ee}, as is given in some recent papers [54].

A Maxwellian distribution of the measured EEPF in the elastic energy range ($\varepsilon < \varepsilon^*$) for ICP at 100 mTorr is due to the overwhelming effect of electron–electron collisions competing with electron cooling due to electron-neutral collisions and electron heating in electromagnetic field. In the absence of electron–electron collisions (at low plasma density) when the electron energy distribution shape is defined by equilibrium between electron heating in rf field and elastic

cooling, the EEPF for $\varepsilon < \varepsilon^*$ in a collisionally dominated argon discharge should be close to a Druyvesteyn distribution unless $\omega \gg \nu_{en}$.

The Maxwellization condition for electrons with $\varepsilon \approx T_e$ is $\nu_{ee} \gg \nu_M$ and $\nu_{ee} \gg \nu_E$, [55] where $\nu_M \approx 2\nu_{en}m/M$ is the characteristic frequency of electron cooling, $\nu_E \approx e\langle E\rangle/m v_{th}$ is the characteristic frequency of electron heating, $\langle E\rangle$ is the Ohmic part of electric field averaged over the plasma volume and $v_{th} = (2T_e/m)^{1/2}$ is the electron thermal velocity. These conditions are well satisfied in the centre of 100 mTorr ICP even for lowest discharge power (12.5 W), although, near the plasma boundary, where plasma density is relatively small, we observe a Druyvesteyn-like EEPF.

With a reduction of argon pressure for a fixed discharge power, plasma density falls while electron temperature grows. These two trends lead to a reduction in electron–electron collision frequency, thus increasing the discharge power and decreasing the maximal electron energy where the EEPF coincides with a Maxwellian.

Calculated characteristic frequencies for argon pressure of 10 and 1 mTorr are presented in figures 16 and 17. Here, the values of ν_{ee} are about 10 times lower at 10 mTorr and about 100 times lower at 1 mTorr than that at 100 mTorr. For both these pressures, the values of ν_{en} are practically independent on discharge power, while values of ω_{eff} differ very little from ω.

Having measured the EEPF in the high-energy range (beyond excitation and ionization energy), we were able to calculate the excitation frequency ν^* and the ionization frequency ν_i. Two excitation frequencies ν_1^* and ν_2^* are shown in figures 16 and 17. ν_1^* represents the sum of excitation rates from the ground state of argon atom to the $3p^5 4s$ excited state manifold, i.e. from ground state to the $^3P_0$ and $^3P_2$ metastable states and to the $^3P_1$ and $^1P_1$ resonance states. The threshold energy for this cross-section is $\varepsilon_1^* = 11.55$ eV. ν_2^* represents the sum of excitation rates to the higher forbidden and allowed states. The threshold energy for this cross-section is taken to be $\varepsilon_2^* = 13.10$ eV. The cross-section data (extend to an energy of 50 eV) for calculation of ν_1^* and ν_2^* were taken from [56].

At all gas pressures in our experiment, the characteristic frequency of gas heating due to electron–atom collisions $\nu_M \approx 2\nu_{en}m/M \ll \nu_i$, ν_1^* and ν_2^*, therefore the values of ν_i, ν_1^* and ν_2^*, presented in figures 16 and 17 represent the relative importance of different electron collisional losses in the electron energy balance. There are also electron energy losses to the wall due to fast electron escape and associated with ion acceleration in the ambipolar and wall sheath field. The wall losses are considerable at low-pressure (and dominate in the ion-free fall regime, at $p \leqslant 1$ mTorr) when electron temperature and relative plasma density at the plasma boundary n_s/n are relatively large.

5.4. Pressure dependence

The evolution of the EEPF over a wide range of argon pressure (starting from 0.3 mTorr up to 300 mTorr) for a fixed discharge power of 50 W is shown in figure 18. The EEPF changes considerably over the wide range of pressure, going from a Maxwellian at relatively high pressure (100 and 300 mTorr) to a three-temperature distribution at low-pressure (0.3, 1.0 and 10 mTorr). Although the EEPF at 100 and 300 mTorr

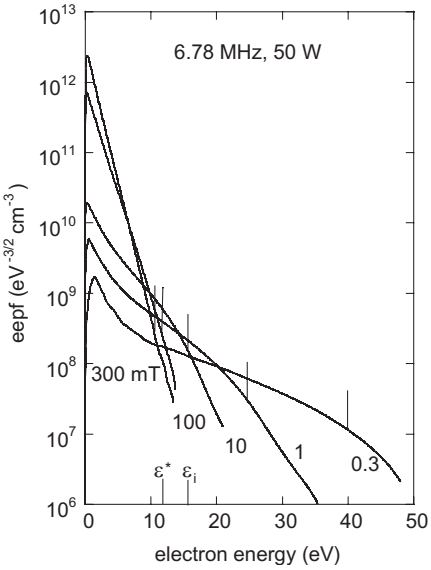

Figure 18. The evolution of the EEPF in a 50 W discharge as gas pressure ranges from 0.3 to 300 mTorr. Vertical lines on the curves show plasma potential.

are accessible only over the elastic energy range ($\varepsilon < \varepsilon^*$), there is no reason to expect a Maxwellian distribution in the inelastic energy range ($\varepsilon > \varepsilon^*$) for these gas pressures. Typically in a gas discharge the EEPF for $\varepsilon > \varepsilon^*$ is essentially depleted, having a differential electron temperature $T_{ed} = -[\mathrm{d}\ln f(\varepsilon)/\mathrm{d}\varepsilon]^{-1}$ less than that in the elastic energy range.

A change in slope of the EEPF in the inelastic energy range is clearly seen at low-pressure where the electron energy interval exceeding the inelastic threshold is accessible. The change in EEPF slope occurs at energy near the threshold of the main mechanism of electron energy loss. For relatively large argon pressures (around 10 mTorr and higher) when excitation is the major electron energy loss process, the change in slope of the EEPF starts near the lowest excitation energy $\varepsilon^* = \varepsilon_1^* = 11.55$ eV (see figure 18 for 10 mTorr). At lower argon pressure (1.0 and 0.3 mTorr) depletion in the EEPF and a change in its slope starts at energy higher than the excitation or ionization energy, ε_1^*, ε_2^* and $\varepsilon_i = 15.76$ eV because fast electron escaping to the wall become the major electron energy loss mechanism in the free fall regime [54]. In figure 18 for low argon pressure, the plasma potential V_p referenced to the grounded chamber wall correlates well with the energy where depletion of the measured EEPFs begins.

It is interesting to note in figure 18 that the plasma potential (i.e. in essence, the floating potential of the metal chamber referenced to the plasma centre) is larger than the excitation energy ε_1^* for low-pressure ICP ($p \leqslant 10$ mTorr). This is a universal feature of non-local electron kinetics [46] and has an important implication for probe diagnostics that use the ion part of the probe characteristic, where electron temperature is inferred from the probe I/V characteristic around the probe floating potential. The electron temperature found in this way is close to the electron differential temperature in the inelastic energy range and is usually smaller than that found through integration of the measured non-Maxwellian EEPF [26]. Moreover, ion current to probe is defined by the screening electron temperature, which is close to the differential electron

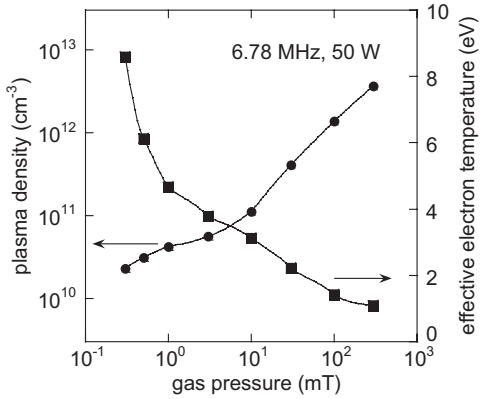

Figure 19. The plasma density and effective electron temperature versus gas pressure for 50 W discharge driven at 6.78 MHz.

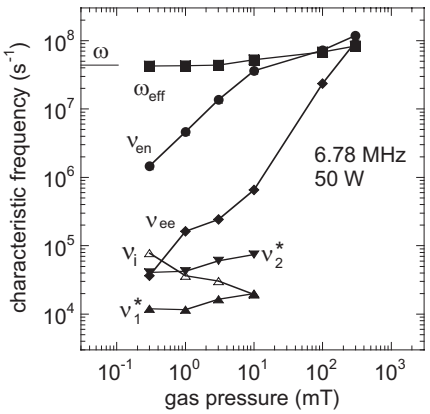

Figure 20. Pressure dependence of characteristic frequencies: ν_{en}, ω_{eff}, ν_{ee}, ν_2^*, ν_1^* and ν_i for a 50 W discharge driven at 6.78 MHz.

temperature for the low energy electrons. As a result, plasma parameters, found from ion current using probe theories derived for Maxwellian electron energy distribution, may be in a large disagreement with those found as integrals of a non-Maxwellian EEPF [26].

The basic plasma parameters, the plasma density n and the effective electron temperature T_e found from integrals of the EEPF are shown in figure 19 as functions of argon pressure. Pressure dependence of plasma density is relatively weak at low-pressure and is nearly linear at higher pressure. The transition from weak to linear dependence occurs at about 10 mTorr and seems to correspond with the evolution from the ion-free fall (Langmuir–Tonks) regime to the ion collisional (diffusion) regime.

The pressure dependence of the electron temperature shown in figure 19 exhibits a pattern typical of gas discharges. As gas pressure decreases (starting from 300 mTorr) there is a slow increase in T_e at relatively high pressure followed by sharp increase when the discharge approaches the threshold of ionization balance instability [54]. This instability occurs due to a slowdown in ionization growth at high electron temperature, when particles loss to the wall grows with electron temperature faster than ionization. The occurrence of this instability is the lower limit of the $p\Lambda$ product where a stable ionization balance of the bounded self-sustained plasma can exist without magnetic confinement ($p\Lambda > p_0\Lambda$). For our discharge chamber filled with argon, we found $p_0\Lambda \approx 1$ mTorr cm.

Pressure dependencies of characteristic frequencies: ω_{eff}, ν_{en}, ν_{ee}, ν_1^*, ν_2^* and ν_i are shown in figure 20. Over a pressure range of three orders of magnitude, the effective rf frequency ω_{eff} rises by a factor of two, being equal to ω at the lowest argon pressure, while the electron–atom transport collision frequency ν_{en} grows linearly with pressure up to 10 mTorr, then grows more slowly. The slowdown in growth is due to a drop in the electron temperature with gas pressure and the strongly pronounced Ramsauer effect in argon. These two effects considerably offset the growth of ν_{en} with gas pressure [43].

On the other hand, at low argon pressure ($p < 10$ mTorr), the ICP electrodynamics are essentially affected by the collisionless (stochastic) electron heating process that can be accounted for by an effective electron collision frequency ν_{eff} including both, collisional and stochastic heating ($\nu_{eff} > \nu_{en}$), [49]. Thus, the Ramsauer effect at relatively high pressure and stochastic electron heating at low-pressure result in an unusually weak dependence of ν_{eff} on argon pressure. The value ν_{eff} has been inferred from the plasma conductivity measurement in the skin layer of our ICP operated between 0.3 and 1000 mTorr using magnetic probes [43]. ν_{eff} was found to increase just 10 times while argon pressure increased 3000 times.

Dependence of the electron–electron collision frequency ν_{ee} on gas pressure is rather complicated and corresponds to the pressure dependence of plasma density and electron temperature shown in figure 19. The frequency of direct ionization ν_i falls with gas pressure (as expected for any self-sustained discharge), while excitation frequencies ν_1^* and ν_2^* grows with gas pressure in the pressure range between 0.3 and 10 mTorr.

5.5. *Frequency dependence*

There are a few ways that the rf frequency may effect ICP operation. First, due to electron inertia, the imaginary part of the plasma conductivity, $\sigma_p = ne^2/m(\nu_{en} + j\omega_{eff})$ transformed to the primary induction coil depends on ω. Together with the reactance of the coil itself, this results in frequency dependence of ICP external electrical characteristics. The frequency effect on real and imaginary part of the induction coil impedance measured in our ICP at frequencies 3.39, 6.78 and 13.56 MHz is reported elsewhere [18]. The imaginary part of rf electric field, due to electron inertia and the coil reactance, both grow with frequency but should not affect ICP ionization and energy balance (and thus, the plasma parameters) provided that the rf power delivered to the plasma is held constant (independent of frequency).

Second, the rf frequency could effect ICP operation due to the frequency dependence of the skin layer depth where electron heating process is localized. An increase in frequency leads to a reduction in skin depth and an enhancement of rf electric field there. This enhancement is mainly due to an increase in the imaginary part of the electric field and, therefore, should not affect the ICP energy balance. A small increase in the Ohmic part of rf field in the skin layer is compensated by the shrinking skin depth, thus it has no

practical effect on the plasma parameters, since non-local electron kinetics ($\lambda_\varepsilon \gg \delta$) in a low-pressure ICP are defined by the volume averaged rf electric field [45–47]. In a high pressure ICP governed by local electron kinetics ($\lambda_\varepsilon \ll \delta$), the frequency dependence of the skin depth may affect local plasma parameters. Here, λ_ε is the electron energy relaxation length, which for an average electron in the elastic energy range can be estimated as: $\lambda_\varepsilon \approx \lambda_{en}(2m/M + \nu_{ee}/\nu_{en})^{-1/2}$. In the inelastic energy range, λ_ε is much shorter and is defined by excitation, ionization and by the wall loss of fast electrons.

Third, rf frequency can affect the electron energy distribution due to collisionless resonant interaction ($\omega = kv_{th}$, k is the wave number) where the phase velocity of an electromagnetic field is near that of the electron thermal velocity. Such a possibility has been discussed many times in connection with helicon plasma sources in an attempt to postulate a highly ionizing electron beam presumably generated by helicon waves in the process of Landau damping. Recent experiments in helicon plasmas [57], where the EEDF was measured with an electrostatic energy analyzer, show no presence of such a fast electron beam.

In an ICP, resonant interaction of the electromagnetic field with plasma electrons ($\omega = kv_{th} \approx v_{th}/\delta$) occurs in the regime of anomalous skin effect when thermal electrons cross the skin layer without collisions in a fraction of an rf period ($v_{th}/\delta > (\omega^2 + \nu_{en}^2)^{1/2}$), [7, 19, 39]. Experimental evidence of collisionless power absorption and its frequency dependence measured in our ICP operating in a nearly collisionless regime (1–10 mTorr) has been reported in [49], while the frequency dependence of the EEPF measured at 3.39, 6.78 and 13.56 MHz has been reported in [12].

EEPFs measured at the plasma centre in a collisionally dominated ($\nu_{en} > \omega$) ICP operating in the normal skin effect regime ($v_{th}/\delta \ll (\omega^2 + \nu_{en}^2)^{1/2}$), corresponding to an argon pressure larger than tens of milliTorr, have shown no significant dependence of the EEPF and plasma parameters on driving frequency. But an essential EEPF dependence on frequency has been found in the nearly collisionless regime [12] as shown in figures 21 and 22 for 1 mTorr and 10 mTorr, respectively.

The frequency dependence of the EEPF is expressed most clearly at the lowest argon pressure and discharge power where the plasma density is relatively small. A rise in argon pressure and discharge power leads to an increase in plasma density, thus, to an enhancement of electron–electron interaction and to Maxwellization of the EEPF in the elastic energy range. Therefore, at relatively large discharge power (200 W and more) and large argon pressure (10 mTorr and more) EEPFs are practically frequency independent.

The two-temperature EEPF structure in elastic energy range seen in figures 21 and 22 is a rather universal feature of low-pressure rf discharges (capacitive, inductive and surface-wave) and is a consequence of non-local electron kinetics of a bounded plasma in a sub-critical ($\omega \ll \omega_{ep}$) electromagnetic field, where ω_{ep} is the electron plasma frequency. In an ICP the main interaction of the electromagnetic field with plasma is localized in skin layer at the plasma boundary that is accessible only to relatively fast electrons that are able to overcome the ambipolar potential. As a result, mainly mid-energy and fast electrons participate in the heating process while low energy electrons are trapped by the dc ambipolar potential in the plasma bulk where the rf field is negligibly small [44].

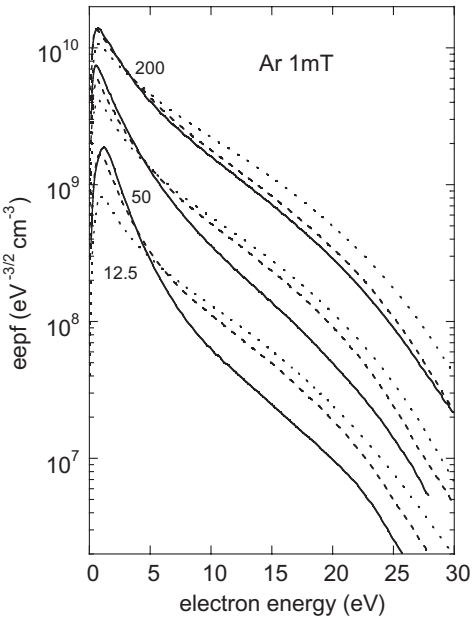

Figure 21. The EEPF versus electron energy for discharge power of 12.5, 50 and 200 W at a gas pressure of 1 mTorr. The solid line represents a driving frequency of 13.56 MHz, the dashed line 6.78 MHz and the dotted line 3.39 MHz.

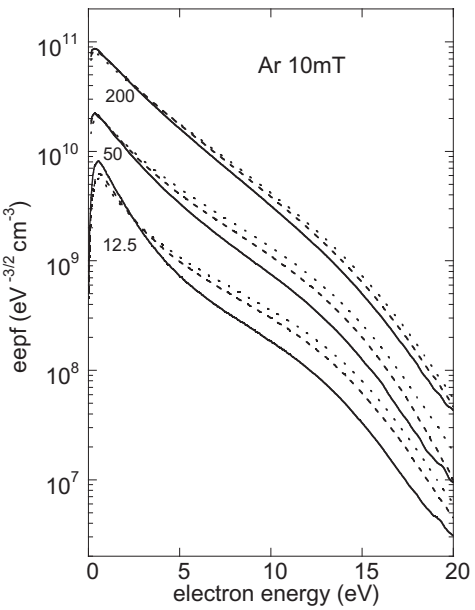

Figure 22. The EEPF versus electron energy for discharge power of 12.5, 50 and 200 W at a gas pressure of 10 mTorr. The solid line represents a driving frequency of 13.56 MHz, the dashed line 6.78 MHz and the dotted line 3.39 MHz.

The energy level ε_1 that divides trapped low energy electrons ($\varepsilon < \varepsilon_1$) from those penetrating the inner boundary of the skin layer ($\varepsilon > \varepsilon_1$) is defined by the ambipolar potential there, V_1, which is considerably smaller than the ambipolar potential at the plasma boundary with the sheath, V_s. For an ion-free path regime (typical for anomalous skin effect), $eV_s \approx T_{es} < T_e$, [50]. Since for the non-Maxwellian EEPFs shown in figures 21 and 22 the screening temperature T_{es} is governed by slow electrons and the skin depth $\delta = 2.0$–2.4 cm

(resulting in $V_1 \approx 1$ V), a considerable portion of plasma electrons interact with the skin layer.

Formation of a two-temperature EEPF and its frequency dependence in an ICP is a direct consequence of collisionless electron heating at the condition of anomalous skin effect [39]. The most efficient energy gain for an electron entering the skin layer and reflected by the sheath back into plasma occurs for electrons that cross the skin layer (back and forth) in a time close to half of an rf period, $v \approx \omega\delta$, otherwise, when $v \ll \omega\delta$, electrons oscillate in the skin layer with no net energy gain, or when $v \gg \omega\delta$, electrons spend too little time in the skin layer to gain energy there. Roughly dividing the slow and fast electrons by the condition $v = \omega\delta$, we can evaluate the critical electron energy $\varepsilon_a = \frac{1}{2}m(\omega\delta)^2$ corresponding to an onset in anomalous collisionless electron heating and to a change in EEPF slope. The critical energy ε_a, corresponding to a change in EEPF slope, was calculated using skin depth data inferred from measurements of the rf electric field distribution in the skin layer [36]. It has been found that $\varepsilon_a \approx 0.65$, 2.5 and 9 eV, correspondingly, for 3.39, 6.78 and 13.56 MHz. These energies seem fairly close to the knee of the EEPFs at the smallest discharge power, when the EEPFs are not smoothed by electron–electron interaction that smears the boundary between slow and fast electron groups. With increasing discharge power the frequency dependence of the EEPF vanishes due to a common trend toward Maxwellization.

Measurements at different frequencies [12] showed that plasma density and electron–atom collision frequency in the discharge centre are not sensitive to the driving frequency, while an essential difference was found in the effective electron temperature calculated through integration of the measured EEPF. An example of pronounced frequency dependence of effective electron temperature is shown in figure 23 for 1 mTorr and for different discharge power.

Probe measurements in a low frequency ICP excited at 0.45 and 0.9 MHz at 1 mTorr [13, 21] reveal a profound change in the EEPF and in corresponding plasma macro parameters (mainly in their spatial distribution) associated with a ponderomotive effect caused by rf Lorentz force. We could not generate a set of EEPFs for a low frequency ICP at low discharge power ($P_d < 100$ W) where (due to negligible electron–electron interaction) changes in the EEPF are expected to be large. Plasma transparency (weak plasma coupling) at such low frequency makes it difficult to sustain an ICP at low discharge power due a loss of ballasting of the ICP driving circuit.

EEPFs and corresponding plasma parameters n and T_e measured in a 200 W ICP at 1 mTorr in a frequency range between 0.45 and 13.56 MHz are presented in figure 24. Disappearance of the low energy peak in the EEPF and a corresponding increase in electron temperature with reduction of driving frequency is clearly seen there. At 0.45 MHz, the EEPF is deficient in low energy electrons, showing a trend toward a Druyvesteyn-like distribution. Over the whole frequency range the plasma density measured in discharge mid-plane has a standard deviation of 0.18, which (accounting for the limited accuracy in plasma density and discharge power measurement) can be considered as frequency independent. A small rise (~30%) in plasma density with a reduction of driving frequency from 13.56 to 0.9 MHz is followed by a small drop at 0.45 MHz. Measurements of the axial plasma density profile for this frequency [14] show a shift in the plasma density maximum outwards from the skin layer due to ponderomotive force.

In an ICP operating at low frequency in a nearly collisionless regime $\varepsilon_a = \frac{1}{2}m(\omega\delta)^2 \ll T_e$. This means that all electrons that penetrate the skin layer participate in the collisionless heating process (in this case the critical energy ε_a, corresponding to a change in the EEPF slope, shifts to zero electron energy). With an increase in argon pressure and discharge power, EEPFs measured at low frequency become Maxwellian and interaction of electromagnetic field with plasma transfers from collisionless to collisional. At this condition the basic plasma parameters T_e and n measured in the plasma centre in the frequency range between 0.45 and 13.56 MHz are found to be very close to each other.

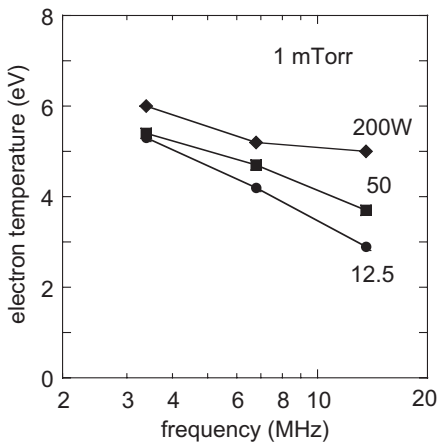

Figure 23. The effective electron temperature versus frequency for discharge power of 12.5, 50 and 200 W at a gas pressure of 1 mTorr.

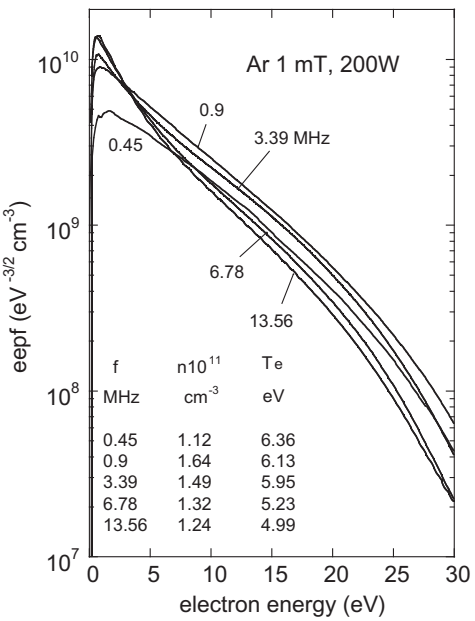

Figure 24. EEPF versus electron energy for five frequencies at a discharge power of 200 W and a gas pressure of 1 mTorr.

6. Conclusion

Analysis of Langmuir probe measurement techniques in high-density plasmas and particularly in ICPs has shown that a large probe circuit resistance is the most common problem and source of error in measurements of EEPFs and inferred plasma parameters of ICP. The rationale behind probe experiment design, to avoid problems associated with the probe circuit resistance as well as problems associated with probe heating, probe contamination and rf interference, is discussed including many details. Using a probe station in which many of the pitfalls of probe measurements are avoided, a comprehensive set of probe measurements have been performed in an ICP to determine EEPF and associated plasma parameters over a wide range of power, gas pressure and frequency.

The measurements were performed in one single system with well-defined discharge geometry and rf power delivered to the plasma. Additionally, plasma parameters inferred here from probe measurements are supplemented with published (elsewhere) external electrical characteristics (coil voltage, coil current and phase between them) and electromagnetic field and current space distributions measured with magnetic probes in the very same ICP system. All these measurements, made over wide range of discharge external and internal parameters in one single system, present a comprehensive database of mutually compatible ICP parameters suitable for validation of theoretical and modelling schemes. The empirical scaling laws for plasma parameters and internal and external electrical characteristics, found in these experiments can be helpful in design of ICP based plasma sources in variety of technological applications.

Acknowledgments

The authors are thankful to A A Sapozhnikov for mechanical design and manufacturing of Langmuir and magnetic probes.

References

[1] Hopwood J, Guarnieri C R, Whitehair S J and Cuomo J J 1993 *J. Vac. Sci. Technol.* A **11** 152
[2] Mahoney L J, Wendt A E, Barrios E, Richards C J and Shohet L J 1994 *J. Appl. Phys.* **76** 204
[3] Kortshagen U, Pukropski I and Zethoff M 1994 *J. Appl. Phys.* **76** 2048
[4] Mumken G and Kortshagen U 1996 *J. Appl. Phys.* **80** 6639
[5] Mumken G 1999 *J. Phys. D: Appl. Phys.* **32** 804
[6] Godyak V A 1996 *Proc. ESCAMPIG 96 (European Phys. Soc., Bratislava, Slovakia, 1996)* vol 20E, Part A, ed Lukac, Kozinar and Skalny, pp IX–XII
[7] Godyak V A 1998 Electron kinetic and electrodynamic characteristics of ICP in stochastic heating regime *Electron Kinetics and Application of Glow Discharges* ed U Kortshagen and L Tsendin (New York: Plenum) p 242
[8] Godyak V A, Piejak R B and Alexandrovich B M 1995 *Plasma Sources Sci. Technol.* **4** 332
[9] Schwabedissen A, Benck E C and Roberts J R 1997 *Phys. Rev.* E **55** 3450
[10] Singh H and Graves D 2000 *J. Appl. Phys.* **87** 4098
[11] Chung C W and Chang H Y 2000 *Phys. Plasmas* **7** 3826
[12] Godyak V A and Kolobov V I 1998 *Phys. Rev. Lett.* **81** 369
[13] Godyak V A, Alexandrovich B M and Kolobov V I 2001 *Phys. Rev* E **64** 026406-1
[14] Godyak V A, Piejak R B, Alexandrovich B M and Smolyakov A I 2001 *Plasma Sources Sci. Technol.* **10** 459
[15] Scheubert P, Frantz U, Awakowicz P and Paulin H 2001 *J. Appl. Phys.* **90** 587
[16] Xu S, Ostrikov K N, Li Y, Tsakadze E L and Jones I R 2001 *Phys. Plasmas* **8** 2549
[17] Godyak V A, Piejak R B and Alexandrovich B M 1992 *Plasma Sources Sci. Technol.* **1** 179
[18] Godyak V A, Piejak R B and Alexandrovich B M 1999 *J. Appl. Phys.* **85** 703
[19] Godyak V A, Piejak R B and Alexandrovich B M 1994 *Plasma Sources Sci. Technol.* **3** 169
[20] Vinogradov G K 2000 *Plasma Sources Sci. Technol.* **9** 400
[21] Godyak V A, Piejak R B, Alexandrovich B M and Smolyakov A I 2000 *Plasma Sources Sci. Technol.* **9** 541
[22] Schott L 1968 *Plasma Diagnostics* ed W Lochte-Holtgreven (Amsterdam: North Holland) p 669, chapter 11
[23] Hershkowitz N 1989 *Plasma Diagnostics* vol I, ed O Auciello and D L Flamm (Boston: Academic Press) p 113
[24] Godyak V A 1990 Measuring EEDF in Gas Discharge Plasmas *Plasma–Surface Interaction and Processing of Materials* vol 179, ed O Auciello *et al (NATO Advance Study Institute, Ser. E)* (Dordrecht: Kluwer) p 95
[25] Godyak V A, Piejak R B and Alexandrovich B M 1992 *Plasma Sources Sci. Technol.* **1** 36
[26] Godyak V A, Piejak R B and Alexandrovich B M 1993 *J. Appl. Phys.* **73** 3657
[27] Sudit I D and Woods R C 1994 *J. Appl. Phys.* **76** 4488
[28] Arslanbekov R R, Khromov N A and Kudryavtsev A A 1994 *Plasma Sources Sci. Technol.* **3** 528
[29] Demidov V I, Kolokolov N B and Kudryavtsev A A 1996 *Probe Diagnostics of Low-Temperature Plasma* (Moscow: Energoizdat) (in Russian)
[30] Bryant P, Dyson A and Allen J E 2001 *J. Phys. D: Appl. Phys.* **34** 1491
[31] Chen F F 2001 *Phys. Plasmas* **8** 3029
[32] Piejak R, Godyak V, Alexandrovich B and Tishchenko N 1998 *Plasma Sources Sci. Technol.* **7** 590
[33] Godyak V A and Popov O I 1977 *Sov. Phys. Tech. Phys.* **22** 461
[34] Godyak V A, Piejak R B and Alexandrovich B M 2001 *Proc. 9th Int. Symp. on the Sci. and Technol. of Light Sources (Ithaca, NY, USA, August 2001)* (Ithaca, NY: Cornell University Press) p 157
[35] Godyak V A and Kolobov V I 1997 *Phys. Rev. Lett.* **79** 4589
[36] Godyak V A and Piejak R B 1997 *J. Appl. Phys.* **82** 5944
[37] Godyak V A and Piejak R B 1998 *J. Phys.* IV France **8** Pr 7-241
[38] Godyak V A, Piejak R B and Alexandrovich B M 1999 *Phys. Rev. Lett.* **83** 1610
[39] Lieberman M A and Godyak V A 1998 *IEEE Trans. Plasma Sci.* **26** 955
[40] Godyak V A, Piejak R B, Alexandrovich B M and Kolobov V I 1999 *Phys. Plasma* **6** 1804
[41] Godyak V A 1986 *Soviet Radio Frequency Discharge Research* (Falls Church, VA: Delphic Associates)
[42] Lieberman M A and Lichtenberg A J 1994 *Principles of Plasma Discharges and Materials Processing* (New York: Wiley) p 137
[43] Godyak V A, Piejak R B and Alexandrovich B M 1999 *J. Appl. Phys.* **85** 3081
[44] Godyak V A and Piejak R B 1990 *Phys. Rev. Lett.* **65** 996
[45] Tsendin L D 1995 *Plasma Sources Sci. Technol.* **4** 200
[46] Kolobov V I and Godyak V A 1995 *IEEE Trans. Plasma Sci.* **23** 503
[47] Kortshagen U, Busch C and Tsendin L D 1996 *Plasma Sources Sci. Technol.* **5** 1
[48] Kolobov V I and Economou D J 1997 *Plasma Sources Sci. Technol.* **6** R1
[49] Godyak V A, Piejak R B, Alexandrovich B M and Kolobov V I 1998 *Phys. Rev. Lett.* **80** 3264
[50] Godyak V A, Meytlis V P and H R Strauss 1995 *IEEE Trans. Plasma Sci.* **23** 728

[51] Lawler J E and Den Hartog E A 1991 *Phys. Rev.* A **15** 4427
[52] Shkarovsky P, Johnson T W and Bachinski M P 1966 *The Particle Kinetics of Plasmas* (Reading, MA: Adison-Wesley)
[53] Spitzer L 1961 *Physics of Fully Ionized Gases* 2nd edn (New York: Interscience)
[54] Granovski L V 1971 *Electrical Current in Gas* ed L A Sena and V E Golant (Moscow: NAUKA) (in Russian)
[55] Davydov B I 1939 *Sow. Phys.* **8** 59
[56] Tachibana K 1986 *Phys. Rev.* A **34** 1007
[57] Blackwell D D and Chen F F 2001 *Plasma Sources Sci. Technol.* **10** 226